Location Aware Resource Allocation for Cognitive Radio Systems and Compressed Sensing based Multiple Access for Wireless Sensor Networks

by

Tong Xue
B.Sc., Southeast University, 2004
M.Sc., Monash University, 2010

A Dissertation Submitted in Partial Fulfillment of the
Requirements for the Degree of

DOCTOR OF PHILOSOPHY

in the Department of Electrical and Computer Engineering

Location Aware Resource Allocation for Cognitive Radio Systems and Compressed Sensing based Multiple Access for Wireless Sensor Networks

by

Tong Xue

B.Sc., Southeast University, 2004

M.Sc., Monash University, 2010

Supervisory Committee

Dr. Xiaodai Dong, Supervisor

(Department of Electrical and Computer Engineering)

Dr. Wusheng Lu, Departmental Member

(Department of Electrical and Computer Engineering)

Dr. Daniela Constantinescu, Outside Member

(Department of Mechanical Engineering)

Supervisory Committee

Dr. Xiaodai Dong, Supervisor

(Department of Electrical and Computer Engineering)

Dr. Wusheng Lu, Departmental Member

(Department of Electrical and Computer Engineering)

Dr. Daniela Constantinescu, Outside Member

(Department of Mechanical Engineering)

ABSTRACT

In this thesis, resource allocation and multiple access in cognitive radio (CR) and compressed sensing (CS)-based wireless networks are studied. Energy-efficiency oriented design becomes more and more important in wireless systems, which motivates us to propose a location-aware power strategy for single user and multiple users in CR systems and a CS-based processing in wireless sensor networks (WSNs) which reduces the number of data transmissions and energy consumption by utilizing sparsity of the transmitted data due to spatial correlation and temporal correlation.

In particular, the work on location-aware power allocation in CR system gives a brief overview of the existing power allocation design in the literature and unifies them into a general power allocation framework. The impact of the network topology

on the system performance is highlighted, which motivates us to propose a novel location-aware strategy that intelligently utilizes frequency and space opportunities and minimizes the overall power consumption while maintaining the quality of service (QoS) of the primary system. This work shows that in addition to exploring the spectrum holes in time and frequency domains, spatial opportunities can be utilized to further enhance energy efficiency for CR systems.

Then the work of resource allocation is extended to finding the power strategy and channel allocation optimization for multiple secondary users in an orthogonal frequency division multiplexing (OFDM) based cognitive radio network. Three different spectrum access methods are considered and utilized adaptively according to the different locations of the secondary users, and we unify these spectrum access methods into a general resource allocation framework. An interference violation test is proposed to decide the parameters in this framework that indicate the set of licensed channels to be sensed. The proposed scheme intelligently utilizes frequency and space opportunities, avoids unnecessary spectrum sensing and minimizes the overall power consumption while maintaining the quality of service of the primary system. The uncertainty of channel state information between the secondary users (SUs) and the primary users (PUs) is also taken into account in the study of power and channel allocation optimization of the SUs. Simulation results validate the effectiveness of the proposed method in terms of energy efficiency and show that enhanced performance can be obtained by utilizing spatial opportunities.

The work on CS-based WSNs considers the application of compressed sensing to WSNs for data measurement communication and reconstruction, where N sensor nodes compete for medium access to a single receiver. Sparsity of the sensor data in three domains due to time correlation, space correlation and multiple access are being utilized. A CS-based medium access control (MAC) scheme is proposed and an in-

depth analysis on this scheme from a physical layer perspective is provided to reveal the impact of communication signal-to-noise ratio on the reconstruction performance. We show the process of the sensor data converted to the modulated symbols for physical layer transmission and how the modulated symbols recovered via compressed sensing. This work further identifies the decision problem of distinguishing between active and inactive transmitters after symbol recovery and provides a comprehensive performance comparison between carrier sense multiple access and the proposed CS-based scheme. Moreover, a network data recovery scheme that exploits both spatial and temporal correlations is proposed. Simulation results validate the effectiveness of the proposed method in terms of communication throughput and show that enhanced performance can be obtained by utilizing the sensed signal's temporal and spatial correlations.

Contents

List of Tables

List of Figures

ACKNOWLEDGEMENTS

Preparing an acknowledgement list is a very enjoyable task. It brings back so many pleasant memories. Truthfully, this thesis would not have been completed without the support and encouragement of so many people. Therefore, I express my sincere gratitude to the following people.

Firstly, I would like to thank my supervisor, Dr. Xiaodai Dong for her expert guidance and generous support throughout my candidature. The regular meetings with her have been very crucial in every step of my research. I earnest appreciate the great amount of time she spent for improving quality of my papers as well as this thesis. Her enthusiasm and integrity will definitely influence me long in my later career. I would also like to thank her for the financial support on my Ph.D program.

I would also like to thank Dr. Wusheng Lu of Department of Electrical and Computer Engineering, for his kindness in providing the course on compressed sensing which is used in the thesis as well as many valuable advices on compressed sensing related issues.

I would also like to thank Dr. Yi Shi, the research work would not be successful without his help. The discussions with him in the early time of my candidature are important and very beneficial. I would also like to thank the University of Victoria especially the Department of Electrical and Computer Engineering for providing me the opportunity for Ph.D study.

Friendship is important, especially when you are away from home. I would not have completed this research without the supports of all my friends. I am so glad to have met all of you. My fellow postgraduates, especially Ted C.K. Liu, Yuzhe Yao, Youjun Fan, Guowei Zhang, Biao Yu, Congzhi Liu, Shuai He, Zheng Xu, Ming Lei, Guang Zeng, Binyan Zhao, Ping cheng, Yuejiao Hui, Leyuan Pan, Yongyu Dai, Wanbo Li, Weiheng Ni, Lan Xu and Le Liang. My friends Quan Zhou, Roger Bian

and Min Gu. Thank you all and I really enjoy the time with you!

My very special thank you goes to my parents and my wife, Jing Zhou. It is your love that supports and encourages me every step of the way.

Tong Xue

University of Victoria

December 2014

DEDICATION

This thesis is dedicated to my family...

Chapter 1

Introduction

In recent years, the design concept of wireless communications is shifting towards energy-efficiency besides capacity and rates, primarily aiming to resolve the escalating overall energy consumption foreseen in the near future. Such a concept is the core component of green communications. Cognitive Radio (CR), thanks to its sensors, is an enabling technology for green communications which enhances the spectrum efficiency and reduces the electromagnetic radiation levels. Compressed sensing (CS), a novel mathematical theory, can also be applied in wireless communication systems to implement green communications. CS acquires a signal of interest indirectly by collecting a relatively small number of observations rather than evenly sampling it at the Nyquist rate which fundamentally changes the traditional digital signal processing in wireless communications and enhances the energy efficiency. Motivated by the benefits of these mentioned technologies, my research work is focused on the sensing and power allocation strategy of CR systems and CS-based wireless sensor networks (WSNs) to hold the promise of green communications. In this chapter, we briefly review the background of CR and energy efficient WSNs, followed by a summary of the contribution of the thesis.

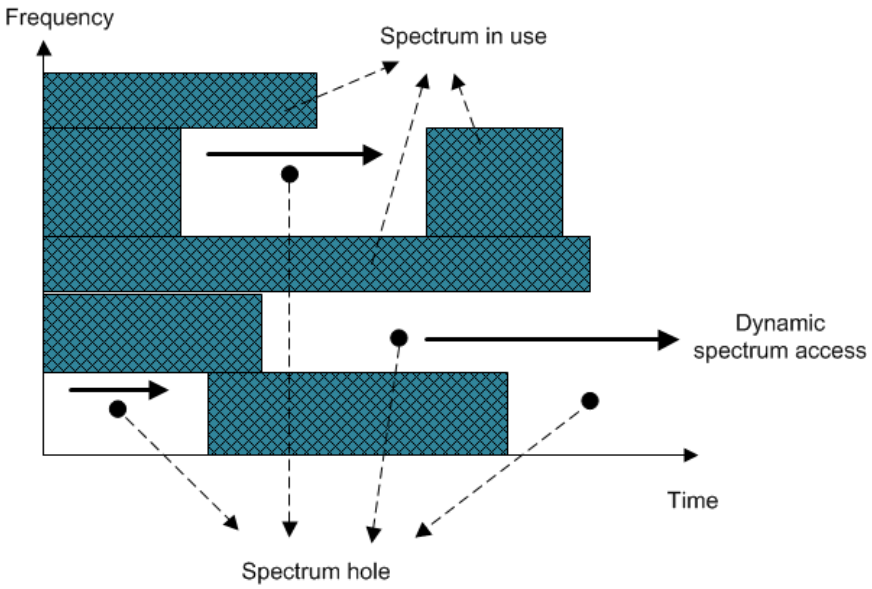

Figure 1.1: Spectrum hole and dynamic spectrum access.

1.1 Cognitive Radio

In November 2002, the Federal Communications Commission (FCC) published a report [1] and it shows that spectrum access is a more significant problem than the physical scarcity of spectrum due to the inflexible spectrum regulation policy. In fact, most of the allocated frequency bands are under-utilized: some frequency bands in the spectrum are largely unoccupied most of the time, and some other frequency bands are only partially occupied [2, 3]. This motivates the rise of CR, which is an intelligent wireless communication system that makes use of spectrum according to its surrounding environment to improve spectrum utilization significantly. In a CR system, it is possible for a SU (not authorized) to utilize the spectrum resource unoccupied by the PU.

Basically, a CR is a radio that can dynamically sense the spectrum and make use of the underused spectrum resource in an opportunistic manner by changing its transmitter parameters. As shown in Fig. 1.1, CR opportunistically accesses the unused spectrum, referred to as *spectrum holes*. The spectrum hole is the frequency resource

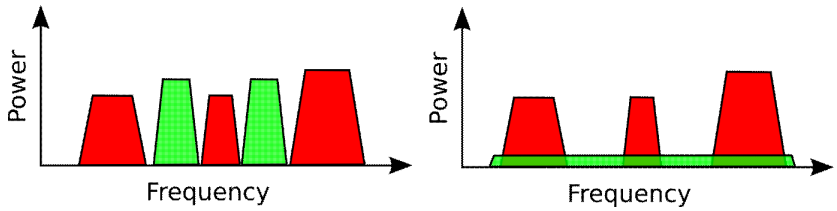

Figure 1.2: Overlay and underlay spectrum access

assigned to PUs, but not being utilized at a particular time or specific geographic location. Spectrum sensing, which monitors the usage of licensed spectra, is a key component required in CR to avoid possible mutual interference between PUs and SUs. There are various spectrum sensing methods, such as matched filter-based detection, energy detection, feature detection, hybrid sensing, cooperative sensing. There exists much research work on spectrum sensing for CR systems, e.g., [4–7]. In [8], the authors give a survey of spectrum sensing methodologies for cognitive radio and an optimal spectrum sensing framework is developed in [7].

Based on the spectrum sensing results, the CR systems need to allocate the spectrum holes to SUs and adopt appropriate transmit power to enhance performance of CR systems meanwhile avoiding harmful interference to PUs. Sensing and power strategy optimization are important research topics in CR systems that hold the promise of advancing green communication. There exist a number of power allocation approaches in the literature. Depending on spectrum policies laid by the primary system, these approaches can be classified as either *overlay-based* where the SUs can utilize the spectrum only when the PU is absent or *underlay-based* where the SUs are allowed to share the spectrum with the PU, see Fig. 1.2. The red and green power represent for transmit power of PUs and SUs, respectively. The left figure is for overlay and for the underlay case, appropriate power control has to be incorporated to avoid unacceptable interference to the primary system. This will be the topic in Chapters 2-4 of this thesis, more details about this area will be introduced later.

1.2 Compressed Sensing-based Wireless Sensor Networks

1.2.1 Compressed Sensing

The compressed sensing theory was proposed by Emmanuel Candes, Terence Tao, and David Donoho around 2005 in [9–12] and several other papers. In 2008, Emmanuel J. Candes and Michael B. Wakin gave a comprehensive introduction to CS in [13], including the fundamentals of sparse signals, incoherent sampling, robustness of CS and applications. In general, compressed sensing acquires a signal of interest indirectly by taking a relatively small number of random projections rather than evenly sampling it at the Nyquist rate.

The current CS theory relies on two principles: sparsity and incoherence. In [13], the principle of sparsity is highlighted as follows.

- Sparsity expresses the idea that the "information rate" of a continuous-time signal may be much smaller than that suggested by its bandwidth.
- A discrete-time signal depends on a number of degrees of freedom which is relatively much smaller than its (finite) length.
- Many natural signals are sparse or compressible in the sense that they have sparse or approximately sparse representations when expressed in an appropriate basis.

References [13] explains the notion of incoherence as follows.

- The sensing vectors must be spread out in the domain in which the object signals are sparse, just as a spike in the time domain is spread out in the frequency domain.

- Incoherence extends the duality between time and frequency.

1.2.2 Energy-efficient Wireless Sensor Networks

Network lifetime is one of the main issues of wireless sensor networks. Typically, the sensor nodes in WSNs are powered by battery. The limited energy for WSNs motivates the research community to improve the energy efficiency for WSNs.

In WSNs, medium access control plays an indispensable role during data transmission. Basically, packet mode medium access methods are adopted in WSNs, e.g., Aloha, slotted Aloha, carrier sense multiple access (CSMA), time division multiple access (TDMA), etc. Since there exist large number of sensor nodes in WSNs, traditional uncoordinated channel access from multiple sensor nodes such as Aloha and CSMA could result in undesirable packet collisions, additional power consumption from retransmissions, and shortened network lifetime. Therefore, energy-efficient and spectral-efficient multiple access are very important designs aspects for wireless sensor networks. Many relevant publications focus on improving the medium access control (MAC) protocol for WSNs to enhance the energy efficiency. For instance, in [14], the authors proposed a MAC protocol named S-MAC to improve the energy efficiency by periodic listen and sleep, collision and overhearing avoidance, and message passing. In [15], the authors proposed a contention-based MAC protocol named T-MAC, which outperforms S-MAC in terms of energy efficiency by introducing an active/sleep duty cycle. Besides, the scheduling problems in WSNs have also been investigated, e.g., time division multiple access (TDMA) scheduling in [16].

Some publications utilize cooperative communication to improve energy efficiency in WSNs. For example, in [17], the authors adopt the cooperative multiple-input and multiple-output (MIMO) and data-aggregation techniques to reduce the energy consumption per bit in WSNs by cooperative communication and reducing the amount

of data for transmission. The authors in [18] compare the energy efficiency of cooperative and non-cooperative transmission schemes in a simple WSN scenario, and point out cooperative schemes are more energy efficient with some constraints. Opportunistic power allocation for WSNs has also been well studied with the purpose of enhancing the network lifetime and energy efficiency, e.g., [19], [20]. The sensor nodes with opportunistic power allocation can adjust their transmit power on the basis of local channel state information and residual energy information.

A typical wireless sensor network contains a large number of sensor nodes, and these sensor nodes usually do not have to transmit data simultaneously. This motivates us to utilize compressed sensing theory on MAC design for WSNs to implement energy-efficient design. In this thesis, we have proposed a CS-based MAC scheme to allow concurrent data transmission, as well as a network data recovery scheme to keep most of the sensor nodes inactive by utilizing spatial and temporal correlations in the sensed data.

1.3 Contributions and Thesis Outline

In CR system, when spectrum sharing is an option, much higher throughput can be achieved by allowing the SUs to underlay with the PUs, performing concurrent transmissions conservatively such that interference generated to the primary system is kept below a prescribed threshold. This motivates us to propose two sharing-based power allocation approaches which will be described in Chapter 2. Meanwhile, the performance of these approaches highly depends on the network topology, which motivates us to propose a location-aware design that incorporates location information to achieve improved energy efficiency. Utilizing the geographical locations of the SUs, the proposed approach intelligently utilizes frequency and space opportunities, mini-

mizes the overall power consumption while maintaining the quality of service of the primary system, and thus contributes toward an optimized system with more efficient energy delivery.

In Chapter 2, we only considered the power allocation for the single SU case. Chapter 3 extends our previous work and we consider multiple SUs in the secondary system and propose an adaptive spectrum access based resource allocation framework taking into account the location information of the SUs. In Chapter 3, we give a general problem formulation that incorporates all the spectrum access methods and switches between different modes by setting the parameters in this formulation. Meanwhile, to achieve an energy-efficient design, we minimize the power consumption with a given date rate requirement in this problem formulation. The utilized resource allocation schemes in our problem formulation involve the hard-decision based approach for overlay spectrum access and the spectrum sharing based approach for underlay spectrum access as well as the sensing-free based approach.

In Chapter 3, we also propose a novel interference violation test to find out the channels that do not need to be sensed and further avoid unnecessary spectrum sensing and hence improve the energy efficiency. Based on the interference violation test result, the proposed location-aware design then incorporates location information to access the spectrum adaptively and achieve improved energy efficiency.

Since the propagation information from SU to PU is difficult to acquire in practice, we propose a multi-user resource allocation framework with channel uncertainty between SU and PU in Chapter 4. Two different approaches are introduced to solve such a resource allocation problem under different assumptions on the uncertain channel information. The simulation results show the tradeoff between energy efficiency and protection for primary user.

In WSNs, the data acquired by sensor nodes while sensing natural phenomenon

usually can be sparsely expressed in a proper domain, e.g., in the frequency domain or the wavelet domain. This observation motivates us to exploit the sparsity of such compressible data to save energy and channel resources. Typically the readings of the sensor nodes have both spatial correlation due to the closeness of sensors and time correlation due to the smooth variations of the real world signal. Moreover, by considering the scenario that in the wireless sensor network only a small portion of transmitters are active at a certain time instant, the aggregated signal from all the transmitters can be viewed as a sparse signal in the dictionary of an identity matrix. This motivates us to propose a CS-based multiple access scheme which is able to tolerate transmission collisions and a network data recovery scheme that exploits both spatial and temporal correlations in Chapter 5.

In Chapter 5, we describe the complete CS-based symbol recovery process in a multiple access channel and investigate the impact of signal-to-noise ratio (SNR) on the accuracy of the CS-based transmission symbol recovery. To reduce the energy for data transmission, we use multiple antennas at the receiver to increase the number of random projections observed by the receiver. Moreover, a detailed performance comparison between CSMA and the proposed CS-based MAC is provided in Chapter 5. Notice that the system structure described in Chapter 5 is a general case and it can also be applied for CS-based cooperative spectrum sensing which contributes to the CR technology.

Finally, the research contributions achieved in the thesis and possible future work are concluded in Chapter 6.

Chapter 2

A Framework for Location-Aware Resource Allocation Strategies in Cognitive Radio Systems

2.1 Introduction

Cognitive radio (CR) has been distinguished as a transforming technology which holds the promise of advancing green communications [21]. By allowing secondary users (SUs) to borrow unused spectrum from primary licensed networks, CR introduces an intelligent system, which can opportunistically select the network and transmission parameters to improve the radio spectrum efficiency and meet the stringent requirements in future wireless networks [2], [22]. This chapter intends to unify and extend contemporary power allocation design in CR systems by incorporating location-aware strategies. We show that in addition to exploring spectrum holes in time and frequency domains, spatial opportunities can be utilized to further enhance energy efficiency for CR systems.

Spectrum sensing is the primary technique employed by the CR system to de-

tect the availability of licensed spectrum and protect the primary system from being harmfully interfered. Depending on spectrum policies laid by the primary system, the power strategies for CR system can be classified as either *overlay-based* where the SUs can utilize the spectrum only when the primary user (PU) is absent or *underlay-based* where the SUs are allowed to share the spectrum with the PU. In the latter case, appropriate power control has to be incorporated to avoid unacceptable interference to the primary system. Typical overlay-based methods include the widely-adopted hard-decision power allocation (HDPA) and the probabilistic power allocation (PPA) proposed in [23]. HDPA is a simple variant of classic waterfilling, which allocates power only over *unoccupied* sub-channels as indicated by sensing results. To account for sensing errors, a probability-based approach, PPA [23], is proposed which considers explicitly the probability of correct detection in the course of power allocation. As a result, sufficient protection to the primary system is guaranteed on an average basis.

2.2 Motivation

In fact, when spectrum sharing is an option, much higher throughput can be achieved by allowing the SUs to underlay with the PUs, performing concurrent transmissions conservatively such that interference generated to the primary system is kept below a prescribed threshold. Two sharing-based approaches are proposed in this work: A sharing-based PPA approach and a sensing-free power allocation (SFPA) approach. Unlike traditional PPA, sharing-based PPA further utilizes those occupied sub-channels with additional protection to the PU. SFPA is motivated from the sensing-free power control described in [24], which always assumes that all the sub-channels are occupied by the primary system, yet still transmits on the whole

spectrum with proper power control.

The performance of the aforementioned approaches highly depend on the network topology, and in particular, the distance between the SU transmitter and the PU receiver. For example, when the SU is close to the PU, spectrum sensing becomes very important in correctly detecting channel availabilities, thus sensing-based approaches should be employed. On the other hand, when the SU is at a distance to the PU, one would expect the possibility of sharing the spectrum without performing spectrum sensing. Based on these observations, in the second part of this work, we propose a location-aware design that incorporates location information to achieve improved energy efficiency.

2.3 A General Problem Formulation

Consider the scenario that one CR system coexists with one primary system, where a mobile SU is communicating with the cognitive base station (CBS) in the uplink and a worst-case PU receiving signals from the primary base station (PBS), as depicted in Fig. 2.1. The hypothetical PU is assumed to lie at the intersection of the PBS service region boundary and the line between the PBS and mobile SU. The problem formulation and analysis thereafter apply similarly to the secondary downlink scenario and hence this chapter focuses on the secondary uplink. We assume that the primary system is an orthogonal frequency division multiplexing (OFDM) based system, with the licensed spectrum being divided into N sub-channels of the same bandwidth with each sub-channel experiencing flat fading. In Fig. 2.1, the circle to the left represents the service range of the primary system and the shaded circle to the right represents that of the CR system. The intersection of the two circles constructs what we call Region 1. The service range of the CR system is further divided into Region 2 and

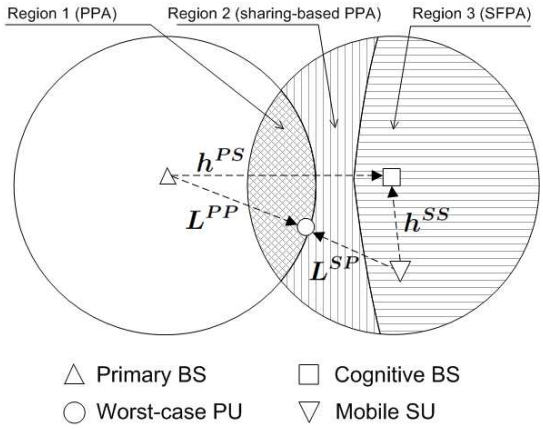

Figure 2.1: A CR system coexisting with a primary system (uplink scenario for the CR system). Three regions are highlighted for the CR system to operate different power allocation strategies.

Region 3. As we shall show, depending on the location of the SU, power allocation design should exhibit an adaptive structure, applying diverse methods when the SU falls into different service regions[1].

In contrast to the popular "maximum design" that maximizes the system data rate over limited power resource [26], we formulate here a complementary quality of service (QoS) problem [27] with the objective of minimizing the overall power consumption subject to a minimum data rate requirement[2]. This formulation is more in agreement with the vision of green communication. Mathematically, the QoS problem for different cognitive power allocation strategies can be formulated by a

[1]The location information of the network can be obtained using, e.g., the cognitive positioning system [25].

[2]These two problems are known to have a primal-dual relationship, but their respective optimal solutions are identical only when the minimum rate threshold in the QoS problem is set equal to the optimal rate value obtained from the maximum design [27].

general framework as[3]

$$
\begin{aligned}
&(\mathbf{P1}) \ \min_{P_i,\forall i} \ \textstyle\sum_{i\in\mathcal{N}_1\bigcup\mathcal{N}_2} P_i \\
&\text{s.t. } R = \sum_{i\in\mathcal{N}_1} \left((1-p_f)\mathcal{C}\left(\tfrac{P_i h_i^{SS}}{\sigma^2}\right) + p_m\mathcal{C}\left(\tfrac{P_i h_i^{SS}}{P_p h_i^{PS}+\sigma^2}\right)\right) + \\
&\quad \alpha\left(\sum_{i\in\mathcal{N}_2}\left(p_f\mathcal{C}\left(\tfrac{P_i h_i^{SS}}{\sigma^2}\right) + p_d\mathcal{C}\left(\tfrac{P_i h_i^{SS}}{P_p h_i^{PS}+\sigma^2}\right)\right)\right) \geq R^{\min} \qquad (2.1)\\
&\quad \textstyle\sum_{i\in\mathcal{N}_1\bigcup\mathcal{N}_2} P_i \leq P^{\max} \qquad (2.2)\\
&\quad p_m P_i L_i^{SP} \leq I_i^{\max}, \qquad \forall i\in\mathcal{N}_1, \qquad (2.3)\\
&\quad \alpha p_d P_i L_i^{SP} \leq I_i^{\max}, \qquad \forall i\in\mathcal{N}_2, \qquad (2.4)
\end{aligned}
$$

where the parameters are explained in Table 2.1, the function $\mathcal{C}(x) = \ln(1+x)$ denotes the Shannon rate, and P_p, p_f, p_m, and p_d are assumed to be known. The average power gains from system A to system B, L^{AB}, are obtained based on path loss attenuation model d^{-r} for a distance d with exponent r, i.e, $L^{AB} = d_{AB}^{-r}$, where d_{AB} denotes the distance between the transmitter in system A to the receiver in system B.

The overlay-based approaches utilize only unoccupied sub-channels based on sensing results and thus the spectrum sharing indicator $\alpha = 0$. To employ the HDPA approach, which ignores sensing imperfections, we can set $p_f = p_m = 0$ and solve problem **P1**. PPA takes into account sensing errors with p_f and p_m determined by sensing accuracy. The underlay-based approaches allow spectrum sharing and thus we have $\alpha = 1$. In particular, we propose the approach of sharing-based PPA in this chapter. Unlike traditional PPA, sharing-based PPA further utilizes those occupied sub-channels with additional protection to the PU. To use this scheme, we need to solve **P1** with the probability information p_f, p_m, and p_d. Note that for PPA and sharing-based PPA, the interference constraint in **P1** guarantees protec-

[3]This formulation can be easily modified to incorporate rate QoS constraint as in [28] and aggregate interference constraint as in [29].

Table 2.1: Parameter Definitions in Problem **P1**

	HDPA | PPA | sharing-based PPA	SFPA
$\mathcal{N}_1$	the set of detected unoccupied sub-channels	N/A ($=\emptyset$)
$\mathcal{N}_2$	the set of detected occupied sub-channels	$\{1, 2, ..., N\}$
p_f	probability of false alarm	N/A ($=0$)
p_m	probability of miss detection	N/A ($=0$)
p_d	probability of detection	N/A ($=1$)
P_i	transmit power allocated on the ith sub-channel of SU	
P_p	transmit power of the PBS	
$R^{\min}$	minimum rate requirement of the CR system	
$P^{\max}$	power budget of SU	
$I_i^{\max}$	QoS threshold of the ith sub-channel for primary system	
h_i^{PS}	instantaneous channel gain on the ith sub-channel from PBS to CBS	
h_i^{SS}	instantaneous channel gain on the ith sub-channel from SU to CBS	
L_i^{SP}	average channel gain on the ith sub-channel from SU to PBS	
σ^2	noise power of each sub-channel at the CBS	
α	spectrum sharing indicator ($\alpha = 0$ for HDPA & PPA and $\alpha = 1$ otherwise)	

tion to the primary system on an average sense. Another underlay-based approach is SFPA, which lets the SU operate on all the sub-channels without spectrum sensing while incorporating the interference constraint (2.4). Therefore, the spectrum sharing indicator $\alpha = 1$ and the other parameters are set according to Table 2.1 with $p_d = 1, p_f = p_m = 0, \mathcal{N}_1 = \emptyset$, and $\mathcal{N}_2 = \{1, 2, ..., N\}$. In a nutshell, different power allocation strategies can be applied by solving **P1** with different sets of parameters.

Problem **P1** is a convex optimization problem and can be infeasible due to the presence of the total power constraint (2.2). This occurs when the total power budget $P^{\max}$ cannot support the target minimum rate $R^{\min}$ for a given channel realization. We can add a slack variable in (2.2) to find the minimum $P^{\max}$ which makes **P1**

feasible [30]. When the problem is feasible, the Lagrangian is given by

$$\mathcal{L} = \sum_{i\in\mathcal{N}_1\bigcup\mathcal{N}_2} P_i + \lambda\left(R^{\min} - R\right) + \mu\left(\sum_{i\in\mathcal{N}_1\bigcup\mathcal{N}_2} P_i - P^{\max}\right) + \sum_{i\in\mathcal{N}_1}\nu_i\left(p_m P_i L_i^{SP} - I_i^{\max}\right) + \sum_{i\in\mathcal{N}_2}\nu_i\left(\alpha p_d P_i L_i^{SP} - I_i^{\max}\right) \quad (2.5)$$

where λ, μ, ν_i are the non-negative Lagrange multipliers. By investigating the Karush-Kuhn-Tucker (KKT) conditions, the optimal solution to **P1** can be derived as

$$P_i = \begin{cases} \left[\frac{1}{2\Theta_1 g_i f_i}\left(-\Theta_1(g_i+f_i) + (1-p_f+p_m)g_i f_i\lambda + \sqrt{(\Theta_1(g_i+f_i) - (1-p_f+p_m)g_i f_i\lambda)^2 - 4\Theta_1 g_i f_i(\Theta_1 - ((1-p_f)g_i + p_m f_i)\lambda)}\right)\right]^+ & \forall i \in \mathcal{N}_1 \\ \left[\frac{1}{2\Theta_2 g_i f_i}\left(-\Theta_2(g_i+f_i) + \alpha(p_f+p_d)g_i f_i\lambda + \sqrt{(\Theta_2(g_i+f_i) - \alpha(p_f+p_d)g_i f_i\lambda)^2 - 4\Theta_2 g_i f_i(\Theta_2 - \alpha(p_f g_i + p_d f_i)\lambda)}\right)\right]^+ & \forall i \in \mathcal{N}_2 \end{cases} \quad (2.6)$$

where $[x]^+ = \max(x, 0)$, $g_i = \frac{h_i^{SS}}{\sigma^2}$, $f_i = \frac{h_i^{SS}}{P_p h_i^{PS} + \sigma^2}$, $\Theta_1 = 1 + \mu + \nu_i p_m L_i^{SP}$ and $\Theta_2 = 1 + \mu + \alpha\nu_i p_d L_i^{SP}$. The Lagrangian multipliers can be numerically computed using the subgradient method [30], based on which P_i can be obtained. Problem **P1** reduces to the classical waterfilling problem when $p_f = p_m = \alpha = 0$. In this case, the corresponding optimal solution, which is given by the first branch of (2.6), becomes $P_i = \left(\frac{\lambda}{1+\mu} - \frac{1}{g_i}\right)^+$.

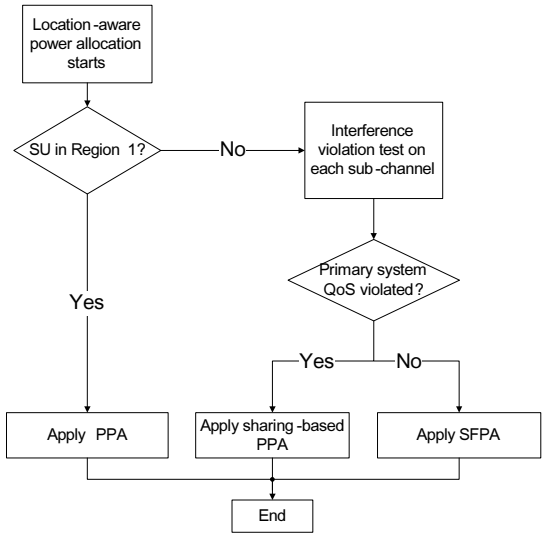

Figure 2.2: The flow chart of the proposed location-aware sensing and power allocation procedure. Please refer to Table I on the specific parameters settings corresponding to different schemes.

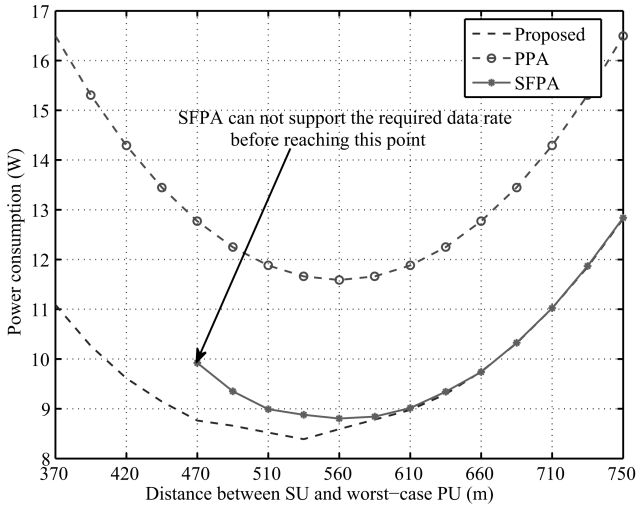

Figure 2.3: Power consumption comparison for different power allocation methods.

2.4 Location-Aware Power Allocation

The proposed scheme is described in the flow chart of Fig. 2.2. For a given network topology, the SU begins with calculating the distance to the PBS and determines if it falls into Region 1. If this is true, the SU will adopt PPA and solve **P1** with $\alpha = 0$. This is because in this region, an SU cannot share the spectrum with the primary

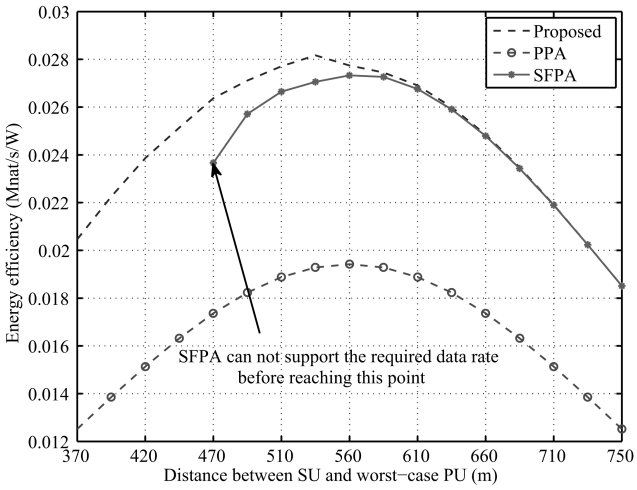

Figure 2.4: Energy efficiency comparison for different power allocation methods.

system based on worst-case design (existence of an infinitely close PU). Otherwise, an interference violation test is activated. In the test procedure, the SU first calculates the traditional water-filling solution without accounting for the interference generated to the primary system. Mathematically, this is equivalent to solving **P1** using SFPA without the interference constraints (2.3) and (2.4). Based on the optimal power allocation results obtained, the amount of interference generated to the PU on each sub-channel is calculated locally and compared to the corresponding QoS threshold. Those sub-channels that are able to support primary system's QoS constitute the sub-channel group that operates the sensing-free strategy, SFPA, whereas for the sub-channels that do violate the interference constraints, we apply sharing-based PPA. This sharing-based PPA approach allows the SU to operate PPA on the unoccupied channels and to share the spectrum with the PU on the occupied channels, achieving higher spectral utilization.

For the purpose of illustration, the boundary of Region 2 and 3 in Fig. 2.1 is obtained based on average channel information, and assuming all the sub-channels obey independent and identically distributed $i.i.d$ Rayleigh fading. In other words, both the instantaneous channel gains h^{PS} and h^{SS} are replaced by their respective

mean values in the process of boundary determination. On the region boundary, the interference constraints (2.3) and (2.4) are satisfied with equalities. In real systems with instantaneous channel information, the sub-channels will have different boundary curves and diverse region patterns. It is affected by system parameters such as the QoS threshold, the minimum data requirement, etc. The region pattern highlights the importance of utilizing location knowledge in achieving adaptive resource allocation, which brings further energy efficiency enhancement to CR systems.

2.5 Numerical Examples

To evaluate the proposed location-aware approach, simulation is conducted for the scenario as shown in Fig. 2.1. Both the service radius of the primary system, R_1, and that of the CR system, R_2, are set to be 1000 m. The coordinates of CBS and PBS are $(0, 0)$ and $(-1500, 0)$, respectively. We assume that the bandwidth of the primary system is 1 MHz, which is divided into 8 sub-channels, each having a bandwidth of 125 kHz. The total path-loss of each transceiver pair is assumed to be affected by both small-scale Rayleigh fading and large-scale path-loss, where the path-loss exponent r is 3. The probability of each sub-channel being unoccupied is 50%, the maximum transmission power of the SU $P^{\max}$ is 20 W, the transmission power of the PBS P_p is 50 W, the minimum data rate requirement $R^{\min}$ is 0.2 Mnat/s, the noise power at CBS σ^2 and the QoS threshold of the primary system $I^{\max}$ are set to be -20 dBmW and -25 dBmW, respectively.

Figs. 2.3 and 2.4 show the power consumption and the corresponding energy efficiency performance, when the SU moves increasingly farther from the primary system along the line segment joint from $(-200, -250\sqrt{3})$ to $(200, -250\sqrt{3})$. The x-axis denotes the distance between SU to the cell-edge PU, which can be calculated

by $d_{SP} = D - R_1$, where D denotes the distance between the SU to the PBS. We define energy efficiency as

$$E = \frac{R_{act}}{\sum_{i \in \mathcal{N}_1 \bigcup \mathcal{N}_2} P_i}, \tag{2.7}$$

where R_{act} is the actual data rate based on a feasible power allocation solution. The equivalent metric for energy efficiency can be found in some publications, e.g., [31]. We notice that for sensing-based approach, we have $R_{act} = R^{\min}$. However, for SFPA, which is based on worst-case design, the actual achieved date rate R_{act} is usually larger than the required data rate, i.e., $R_{act} > R^{\min}$.

The results in Figs. 2.3 and 2.4 are obtained by averaging over a same set of random channel realizations for each value of d_{SP}. In both figures, the performance curves of the proposed location-aware approach are compared with those of the PPA and the SFPA methods under perfect sensing. The curves for the case of imperfect sensing have similar trends, which have not been shown here due to space limitation. As can be observed from both figures, when the SU is close to the worst-case PU ($d_{SP} < 470$ m), the interference constraints translate into very stringent transmit power constraints, so that SFPA provides no solution to guarantee the minimum data rate requirement. As the SU moves away from the PU, the energy efficiency curves for both SFPA and PPA increase rapidly, attaining the maximum value when the SU is closest to the CBS ($d_{SP} = 560$ m). We also observe that the location-aware approach is strictly superior to PPA in terms of both power consumption and energy efficiency, and coincides with SFPA when the SU is sufficiently far from the PU. In summary, the proposed method is able to adapt to different sensing and power allocation strategies at different locations and achieves the minimum power consumption and maximal energy efficiency in all scenarios.

2.6 Conclusion

This chapter has elaborated the role of cognitive radio in advancing green radio communication, by firstly giving an overview of the state-of-the-art research activities in power allocation for OFDM-based CR networks. We have identified the pros and cons of several existing schemes and have proposed a location-aware approach that allows the SU to maximize energy efficiency by adapting to spectrum and spatial opportunities. The proposed approach demonstrates great potential in significantly enhancing the energy-efficiency over the contemporary designs and holds the promise of spearheading the green evolution in future wireless communication systems.

Chapter 3

Resource Allocation Strategy for Multi-user Cognitive Radio Systems: Location-Aware Spectrum Access

In the previous chapter, we studied the location-aware power allocation problem for CR systems considering only a single secondary user. However, for the multiple secondary user case, the general power allocation framework proposed in Chapter 2 can not be used directly since not only power allocation but also channel allocation have to be considered. Therefore, in this chapter we will present a new framework and propose some novel algorithms to solve the resource allocation problem for the multi-user case.

3.1 Introduction

In Chapter 2, we have introduced that the dynamic spectrum access mechanism can be generally classified as overlay spectrum access and underlay spectrum access depending on the spectrum policies laid by the primary system. In an overlay-based

system, the SUs access the spectrum only when it is not being used by the primary system [32] while in an underlay-based system, the SUs coexist with the primary system and transmit with power constraints to avoid unacceptable interference and guarantee the quality of service (QoS) of the primary system [33], [34].

Recently, power and channel allocation in orthogonal frequency-division multiplexing (OFDM)-based CR systems have received a great deal of attention [23, 28, 35–40]. In either overlay-based systems or underlay-based systems, many resource allocation strategies have been proposed in these works. We have introduced overlay-based strategies in Chapter 2, such as hard-decision resource allocation (HDRA) and probabilistic resource allocation (PRA). For the underlay-based system, the interference management among the SUs and the primary users (PUs) play a key role in the resource allocation. In order to protect the primary system, most literatures constrain the interference caused by the SUs below a threshold in either average (long term) or instantaneous (short term) sense, e.g., [33], [41] and [28]. Unlike the previous literature that takes into account the amount of interference to the primary system as the protection criterion, the authors of [38] reconsider the protection to the primary system and SUs through different levels of protection in signal to interference-and-noise ratio (SINR). Besides, many researchers consider the resource allocation with joint overlay and underlay spectrum access. For instance, subcarrier-and-power-allocation schemes for a joint overlay and underlay spectrum access mechanism are proposed in [35] for a downlink transmission scenario in a centralized multi-user CR network, where both unused and underused spectrum resources are utilized and the interference introduced to the PU is kept below given thresholds with a certain probability. In [39], the authors employ a hybrid overlay/underlay spectrum sharing scheme for a distributed CR network, allowing the SU to adapt its way of accessing the licensed spectrum according to the status of the channel. If the selected channel is

detected to be unoccupied, the SU works in an overlay mode, otherwise it works in spectrum underlay. An auction-based power allocation scheme is proposed as well to solve power competition of multiple SUs. All these works mentioned are based on the maximum data rate design subject to an overall power constraint. On the other hand, energy-efficient design attracts the attention from the researchers recently. The energy-efficient power allocation problem of OFDM-based CR systems is studied in [40], where the energy efficiency is taken as the objective function in the optimization for the purpose of holding the promise of advancing green communications.

3.2 Motivation and Contribution

All the existing work aforementioned studied the resource allocation based on spectrum sensing results, and assumed the SUs work with the overlay, underlay or joint overlay/underlay mechanism. However, space opportunity was not considered in most of the existing work which can enhance the spectrum and energy efficiency. In our previous work [42] which has been presented in the previous chapter, a novel location-aware power allocation framework that intelligently utilizes frequency and space opportunities of the spectrum was proposed. A number of power allocation approaches were unified and adopted adaptively according to the location information of the SU. However, in that work, we only considered the power allocation for the single SU case. This chapter extends to consider multiple SUs in the secondary system and propose an adaptive spectrum access based resource allocation framework taking into account the location information of the SUs. In this chapter, we give a general problem formulation that incorporates all the spectrum access methods and switches between different modes by setting the parameters in this formulation. To be differ-

ent from the single user case, channel allocation parameter should be involved in this formulation. Meanwhile, to achieve an energy-efficient design, we minimize the power consumption with a given date rate requirement in this problem formulation. The utilized resource allocation schemes in our problem formulation involves the hard-decision based approach for overlay spectrum access and the spectrum sharing based approach for underlay spectrum access as well as the sensing-free based approach [24]. The performance of the aforementioned approaches highly depends on the network topology, and in particular, the distance between the SU transmitter and the PU receiver. For example, as shown in Fig. 3.1, when the SUs are close to the PU (located in the Overlay Region), spectrum sensing becomes very important in correctly detecting channel availabilities, thus sensing-free schemes can not be employed. On the other hand, when the SUs are at a distance to the PU, one would expect the possibility of sharing the spectrum without the need to perform spectrum sensing. In general, it is not straightforward to decide whether spectrum sensing for each channel is required or not even if the location information is known. Therefore, in this chapter we propose a novel interference violation test to find out the channels that do not need to be sensed and further avoid unnecessary spectrum sensing and hence improve the energy efficiency. Based on the interference violation test result, the proposed location-aware design then incorporates location information to access the spectrum adaptively and achieve improved energy efficiency.

There are several problems in designing resource allocation for the multi-user case. We identify and summarize the two main challenges as well as the contributions of this work as follows:

- *Optimization algorithm for multi-user system*: The optimization algorithm would be more complicated compared to the single user case, since we not only consider the power allocation for certain individual user, but also the channel allocation

for all the users. The optimization problem is no longer a straightforward convex optimization. Thus, in this work, we propose an iterative algorithm based on *time-sharing* condition introduced by [43] to obtain the optimal resource allocation (cf. Algorithm 1).

- *Energy for spectrum sensing*: Unnecessary spectrum sensing leads to extra energy consumption. As mentioned previously, for the SUs being far away, spectrum sensing is a waste of energy. Therefore, a novel adaptive resource allocation algorithm based on an interference violation test is proposed in this chapter for those SUs located far away from the primary system to decide the parameter settings in the general problem formulation. The proposed algorithm helps the SUs utilize the optimal resource allocation scheme and decide whether spectrum sensing is necessary to further enhance the energy efficiency of this system (cf. Algorithm 2).

3.3 System Model and Problem Formulation

3.3.1 Overall Description and Assumptions

This chapter considers a scenario that one CR system coexists with one primary system, where K mobile SUs are communicating with the cognitive base station (CBS) in the uplink and the corresponding worst-case PUs receiving signals from the primary base station (PBS), as depicted in Fig. 3.1. To demonstrate the efficacy of the scheme proposed in this chapter, we assume the worst case location of a PU (being located at the intersection of the PBS service region boundary and the line between the PBS and the relevant mobile SUs) as shown in Fig. 3.1. We believe that if the worst case PU is protected, all the PUs within the coverage area of the primary system are also protected. The problem formulation and analysis thereafter apply

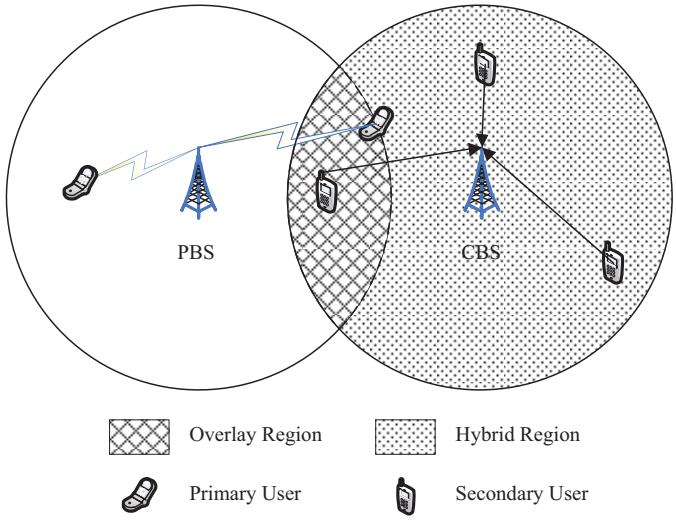

Figure 3.1: A CR system coexisting with a primary system (uplink scenario for the CR system). Two regions are highlighted for the CR system to operate different resource allocation strategies.

similarly to the secondary downlink scenario and hence this paper focuses on the secondary uplink. We assume that the primary system and CR system are OFDM-based systems, with the licensed spectrum being divided into N sub-channels of the same bandwidth with each sub-channel experiencing flat fading. In Fig. 3.1, the circle to the left represents the service range of the primary system and the shaded circle to the right represents that of the CR system. The intersection of the two circles forms what we call Overlay Region. The remaining part of the CR service region is called Hybrid Region. As we shall show, depending on the location of the SUs, resource allocation design should exhibit an adaptive structure, applying diverse methods when the SUs fall into different service regions. In order to avoid mutual interference among SUs, we assume that each sub-channel can be at most allocated to one SU and each SU may be allocated more than one sub-channel. Therefore, channel allocation will be considered in addition to power allocation and we assume that the CBS coordinates the resource allocation and spectrum sensing (if necessary) in a centralized manner.

3.3.2 Problem Formulation and Notations

Transmit power control plays an important role in energy efficient communication to prolong the lifetime of the network and achieve the goal of green communication. Therefore, instead of maximizing the system data rate over limited power resource [26] as most of the relevant works do, we formulate here a complementary QoS problem [27] with the objective of minimizing the overall power consumption subject to a minimum data rate requirement. The QoS problem for different cognitive power allocation strategies can be formulated by a general framework as

$$
\begin{aligned}
&(\mathbf{P1}) \quad \min_{P_{i,k},\rho_{i,k}\forall i,k} \ \textstyle\sum_{k=1}^{K}\sum_{i\in\mathcal{A}\bigcup\mathcal{N}}\rho_{i,k}P_{i,k} \\
&\text{s.t. } R_k = \sum_{i\in\mathcal{A}}\rho_{i,k}\mathcal{C}\left(\frac{P_{i,k}h_{i,k}^{SS}}{\sigma^2}\right) \\
&+\alpha^{(k)}\sum_{i\in\mathcal{N}}\rho_{i,k}\mathcal{C}\left(\frac{P_{i,k}h_{i,k}^{SS}}{\sigma^2+P_p h_i^{PS}}\right) \geq R^{\min}, \forall k \qquad (3.1) \\
&\textstyle\sum_{i\in\mathcal{A}\bigcup\mathcal{N}}\rho_{i,k}P_{i,k} \leq {P_k}^{\max}, \forall k \qquad (3.2) \\
&\alpha^{(k)}\rho_{i,k}P_{i,k}L_{i,k}^{SP} \leq I_i^{\max}, \qquad \forall i\in\mathcal{N}, \forall k, \qquad (3.3) \\
&\sum_{k=1}^{K}\rho_{i,k} \leq 1, \rho_{i,k}\in\{0,1\}, \forall k, i, \qquad (3.4)
\end{aligned}
$$

where the parameters are explained in Table I, the function $\mathcal{C}(x) = \log_2(1+x)$ denotes the Shannon rate, the bandwidth of each sub-channel is assumed to be unitary, the minimum data requirements for all the users are assumed to be identical and P_p is assumed to be known. The average channel gains from system A to system B, L^{AB}, are obtained based on path loss attenuation model d^{-r} for a distance d with exponent r, i.e, $L^{AB} = d_{AB}^{-r}$, where d_{AB} denotes the distance between the transmitter in system A to the receiver in system B. The overlay-based approaches utilize only unoccupied sub-channels based on sensing results and thus the spectrum sharing

Table 3.1: Parameter Definitions in Problem **P1**

	Overlay	Underlay	SFRA
$\mathcal{A}$	the set of detected unoccupied sub-channels		N/A ($=\emptyset$)
$\mathcal{N}$	the set of detected occupied sub-channels		$\{1, 2, ..., N\}$
$P_{i,k}$	transmit power allocated on the ith sub-channel for the kth SU		
P_p	transmit power of the PBS		
$R^{\min}$	minimum rate requirement of the SUs		
$P_k{}^{\max}$	power budget of the kth SU		
$I_i^{\max}$	QoS threshold of the ith sub-channel for the primary system		
h_i^{PS}	instantaneous channel gain on the ith sub-channel from PBS to CBS		
$h_{i,k}^{SS}$	instantaneous channel gain on the ith sub-channel from the kth SU to CBS		
$L_{i,k}^{SP}$	average channel gain on the ith sub-channel from the kth SU to PBS (path loss and shadowing)		
σ^2	noise power of each sub-channel at the CBS		
$\alpha^{(k)}$	spectrum sharing indicator of the kth SU($\alpha^{(k)}=0$ for overlay and $\alpha^{(k)}=1$ otherwise)		
$\rho_{i,k}$	channel allocation indicator ($\rho_{i,k}$=1 represents allocating the ith sub-channel to the kth SU)		

indicator $\alpha^{(k)} = 0$. The underlay-based approaches allow spectrum sharing and thus we have $\alpha^{(k)} = 1$. Unlike traditional overlay systems, underlay-based systems further utilize those occupied sub-channels with additional protection to the PUs. Note that for underlay-based systems, the interference constraint (3.3) in **P1** guarantees protection to the primary system on an average sense and hence supports primary system QoS. Another resource allocation scheme is sensing-free resource allocation (SFRA), which lets the SUs operate on all the sub-channels without spectrum sensing while incorporating the interference constraint (3.3). Therefore, the spectrum sharing indicator $\alpha = 1$ and the other parameters are set according to Table I with $\mathcal{A} = \emptyset$, and $\mathcal{N} = \{1, 2, ..., N\}$.

In this work, for each SU, depending on its location, one of the three resource allocation schemes may be applicable. In a nutshell, the problem **P1** should be

solved considering different sets of parameters for different SUs, with details given in the next sections.

3.4 Location-Aware Multi-User Resource Allocation

With the location information of the SUs, the key part of the proposed resource allocation scheme in this work is selecting the appropriate parameters for **P1** and solving it. In this section, we focus on solving **P1** with the assumption that all the parameters have been determined.

Problem **P1** can be infeasible due to the presence of the total power constraint (3.2) and interference constraint (3.3). This occurs when the total power budget ${P_k}^{\max}$ cannot support the target minimum rate $R^{\min}$ for a given channel realization. When **P1** is feasible, it can not be solved directly since it is a non-convex problem. To solve **P1**, we utilize the dual decomposition approach [43] and the dual problem of **P1** can be given as

$$\begin{aligned} (\mathbf{P2}) \qquad & \underset{\mu}{\text{maximize}} \quad \min_{P_{i,k},\rho_{i,k}\forall i,k} \mathcal{L} \\ & \text{s.t.} \qquad\quad \boldsymbol{\mu_k} \succeq 0, \end{aligned} \tag{3.5}$$

where $\boldsymbol{\mu_k}$ is a vector of non-negative Lagrangian multipliers for user k and $\mathcal{L}$ is the Lagrangian and it is given by

$$\mathcal{L} = \sum_{k=1}^{K} \sum_{i \in \mathcal{A} \bigcup \mathcal{N}} \rho_{i,k} P_{i,k} + \sum_{k=1}^{K} \mu_{1,k} \left(R^{\min} - R_k \right) \tag{3.6}$$

$$+ \sum_{k=1}^{K} \mu_{2,k} \left(\sum_{i \in \mathcal{A} \bigcup \mathcal{N}} \rho_{i,k} P_{i,k} - {P_k}^{\max} \right) \tag{3.7}$$

$$+ \sum_{i \in \mathcal{N}} \mu_{3,i} \left(\alpha^{(k)} \rho_{i,k} P_{i,k} L_{i,k}^{SP} - I_i^{\max} \right) \tag{3.8}$$

$$+ \sum_{i \in \mathcal{A}} \mu_{4,i} \sum_{k=1}^{K} \left(\rho_{i,k} - 1 \right). \tag{3.9}$$

Since **P1** is not convex, the dual problem **P2** provides a solution, which is an upper bound to the solution of **P1**. The upper bound is not always tight, and the difference between the upper bound and the true optimum is called the "duality gap." When the duality gap is zero, they have identical solutions. To show the duality gap between **P1** and **P2** is zero, we first introduce the definition of *time-sharing* condition [43].

Definition 1.[1] Let $P1_{i,k}^*$ and $P2_{i,k}^*$ be optimal solutions to the optimization problem **P1** with $R^{\min} = {R_1}^{\min}$ and $R^{\min} = {R_2}^{\min}$, respectively (for $\forall i, k$). The corresponding channel allocation results are $\rho_{1i,k}$ and $\rho_{2i,k}$, respectively. An optimization problem of the form **P1** is said to satisfy the time-sharing condition if for any ${R_1}^{\min}$, ${R_2}^{\min}$ and for any $0 \leq v \leq 1$, there always exists a feasible solution $P_{i,k}^*$ and channel allocation $\rho_{i,k}$ such that for $\forall k$, $R_k(P_{i,k}^*, \rho_{i,k}) \geq v{R_1}^{\min} + (1-v){R_2}^{\min}$, and $\sum_{k=1}^{K} \sum_i \rho_{i,k} P_{i,k}^* \leq v \sum_{k=1}^{K} \sum_i \rho_{1i,k} P1_{i,k}^* + (1-v) \sum_{k=1}^{K} \sum_i \rho_{2i,k} P2_{i,k}^*$.

Then we have the lemma as shown below:

Lemma 1. The optimization problem **P1** satisfies the time-sharing property when the data rate requirements for all the users are identical, and it has a zero

[1] In Definition 1, constraints (3.2) and (3.3) are not considered since **P1** is assumed to be feasible with satisfied QoS, and interference control is discussed in the next section.

duality gap, i.e., the primal problem **P1** and the dual problem **P2** have the same optimal value.

Proof: When the data rate requirements for all the users are identical, the channel allocation results $\rho_{i,k}$ remain constant as $R^{\min}$ varies. For each $R^{\min}$, R_k is a summation of some logarithmic functions of the allocated power. Thus, it is straightforward that for the optimal power solution, R_k is a concave function of the optimal overall power consumption of user k with any channel allocation result. For **P1**, with the optimal power allocation, the achieved data rate is actually equal to the minimum data rate requirement. Therefore, for any $0 \leq v \leq 1$, $R_k(P^*_{i,k}) \geq v{R_1}^{\min} + (1-v){R_2}^{\min}$ when $\sum_i \rho_{i,k} P^*_{i,k} = \sum_i \rho_{1i,k} v P1^*_{i,k} + \sum_i \rho_{2i,k}(1-v) P2^*_{i,k}$.

This implies that **P1** satisfies the time-sharing property. From [43], if the optimization problem satisfies the time-sharing property, then it has a zero duality gap which completes the proof. □

Problem **P2** can be decomposed into two layers of subproblems. In the lower layer,

$$\begin{aligned} \underset{P_{i,k},\rho_{i,k}\forall i,k}{\text{minimize}} \quad & U \\ \text{s.t.} \quad & \rho_{i,k} \in \{0,1\}, P_{i,k} \geq 0, \end{aligned} \tag{3.10}$$

where $\mathcal{L} = U + V$ and U represents all the terms of L that include $\rho_{i,k}, P_{i,k}$. Let U^* be the minimum value of the objective function in the lower layer, the master problem in the upper layer is

$$\begin{aligned} \underset{\mu}{\text{maximize}} \quad & U^* + V \\ \text{s.t.} \quad & \mu_{\mathbf{k}} \succeq 0. \end{aligned} \tag{3.11}$$

For certain channel i, we can compute the optimal $u^*_{i,k}$ for the kth SU in the lower layer as

$$\begin{aligned} u^*_{i,k} = P_{i,k} - \mu_{1,k} \log_2(1 + \frac{P_{i,k} h^{SS}_{i,k}}{\sigma^2}) + \mu_{2,k} P_{i,k} \\ + \mu_{3,i} P_{i,k} L^{SP}_{i,k} + \mu_{4,i}, \end{aligned} \tag{3.12}$$

where $\sum_{i \in \mathcal{A} \bigcup \mathcal{N}} u^*_{i,k} = U^*$. When the ith channel is allocated to the kth SU, i.e., $\rho_{i,k} = 1$, the power allocation can be determined in a water-filling fashion such that

$$P_{i,k} = \left(\frac{\mu_{1,k}}{(1 + \mu_{2,k}) \ln 2} - \frac{\sigma^2}{h^{SS}_{i,k}} \right)^+. \tag{3.13}$$

Then for any channel, $\rho_{i,k}$ is chosen to be 1 for the user having the minimal $u^*_{i,k}$ which is calculated by substituting $P_{i,k}$ obtained through (3.13) into (3.12). To obtain the Lagrangian multipliers in the lower layer, we can use the subgradient method introduced by [43] to update the multipliers as below:

$$\mu^{(j+1)}_{1,k} = \left(\mu^{(j)}_{1,k} + s^{(j)} (R^{\min} - R_k) \right)^+, \tag{3.14}$$

$$\mu_{2,k}^{(j+1)} = \left(\mu_{2,k}^{(j)} + s^{(j)} (\sum_{i \in \mathcal{A} \bigcup \mathcal{N}} \rho_{i,k} P_{i,k} - {P_k}^{\max}) \right)^{+}, \tag{3.15}$$

$$\mu_{3,i}^{(j+1)} = \left(\mu_{3,i}^{(j)} + s^{(j)} (\alpha^{(k)} \rho_{i,k} P_{i,k} L_{i,k}^{SP} - I_i^{\max}) \right)^{+}, \tag{3.16}$$

where $s^{(j)}$ represents a sequence of step sizes and each value should be sufficiently small [44]. When we update the Lagrangian multipliers, the power allocation solutions are obtained by setting $\rho_{i,k} = 1$. Therefore, $\mu_{4,i}$ is actually not necessary which can be initialized to be 0 and does not need to be updated. Note that we focus on the secondary uplink scenario in this paper, and the power and channel allocation is conducted by the CBS in a centralized manner. The process for solving **P1** can be summarized in Algorithm 1 as shown below.

Algorithm 1 Solving **P1**

Require:

$\mathcal{A}$ = unoccupied channels, $\mathcal{N}$ = occupied channels;
$\mu_{1,k}$, $\mu_{2,k}$ and $\mu_{3,i}$;
${P_k}^{\max}$, $R^{\min}$, ${I_i}^{\max}$;

Ensure:

1. For each user k, calculate $P_{i,k}$ according to (3.13) and $u_{i,k}^{*}$ according to (3.12), respectively.
2. Allocate the channel i to the user having the minimal $u_{i,k}^{*}$ and update $\mu_{3,i}$ according to (3.16).
3. With the channel allocation result, update $\mu_{1,k}$ and $\mu_{2,k}$ according to (3.14) and (3.15), respectively.

Until

the Lagrangian multipliers converge.

Lastcon:

Optimal solution $\mathbf{P}$ and $\rho_{i,k}$;

3.5 Adaptive Resource Allocation with Interference Violation Test

Before solving **P1**, the CBS should decide the parameters that indicate the adopted spectrum access method for each SU. For instance, one of the key points of the proposed scheme is to determine the $\mathcal{A}$ and $\mathcal{N}$ before solving **P1**, which can be obtained by spectrum sensing. However, if an SU is in the Hybrid Region, SFRA may be applicable and in this case, spectrum sensing is unnecessary and $\mathcal{A}$ and $\mathcal{N}$ are selected according to Table I.

For a given network topology, each SU begins with calculating the distance to the PBS and determines if it falls into the Overlay Region. If this is true, the channels allocated to such an SU should be sensed as unoccupied channels, and the SU can only adopt overlay-based spectrum access. This is because in this region, an SU cannot share the spectrum with the primary system based on the worst-case design (existence of an infinitely close PU). If there exists an SU that falls into the Hybrid Region, an interference violation test should be activated. Since SFRA can be a choice to avoid unnecessary spectrum sensing, this interference violation test is conducted to find out the parameter settings in **P1** for SFRA users.

The interference violation test is based on the fact that, if the primary system QoS can be maintained (constraint (3.3) in **P1** holds) regardless whether the respective channels are occupied or not, it is not necessary to perform spectrum sensing. To be more specific, in the test procedure, the coordinator (CBS) first calculates the traditional water-filling solution without accounting for the interference generated to the primary system by solving **P3**.

$$
\begin{aligned}
&(\mathbf{P3}) \quad \min_{P_{i,k},\rho_{i,k}\forall i,k} \ \textstyle\sum_{k=1}^{K}\sum_{i\in\mathcal{A}\bigcup\mathcal{N}}\rho_{i,k}P_{i,k} \\
&\text{s.t. } R_k = \sum_{i\in\mathcal{A}}\rho_{i,k}\mathcal{C}\left(\frac{P_{i,k}h_{i,k}^{SS}}{\sigma^2}\right) \\
&+\sum_{i\in\mathcal{N}}\rho_{i,k}\mathcal{C}\left(\frac{P_{i,k}h_{i,k}^{SS}}{\sigma^2+P_p h_i^{PS}}\right) \geq R^{\min}, \forall k \qquad (3.17) \\
&\textstyle\sum_{i\in\mathcal{A}\bigcup\mathcal{N}}\rho_{i,k}P_{i,k} \leq {P_k}^{\max}, \forall k \qquad (3.18) \\
&\rho_{i,k}P_{i,k}L_{i,k}^{SP} \leq I_i^{\max}, \qquad \forall i \in \mathcal{V} \qquad (3.19) \\
&\sum_{k=1}^{K}\rho_{i,k} \leq 1, \rho_{i,k} \in \{0,1\}, \forall k, i, \qquad (3.20)
\end{aligned}
$$

where $\mathcal{V}$ is a channel set representing those sub-channels that can not support primary system QoS, and at the beginning of the interference violation test, $\mathcal{V}$ is initialized to $\emptyset$. Mathematically, solving **P3** is equivalent to solving **P1** by using SFRA for those SUs located in the Hybrid Region with the interference constraints only for sub-channels belonging to $\mathcal{V}$, and using the overlay strategy for those SUs located in the Overlay Region. It is worth noting that the $I_i^{\max}$ for the channel allocated to the SUs located in the Overlay Region should be set to 0, and thus the according channel must be sensed. With the obtained power and channel allocation results, the generated interference to PUs will be checked to find out whether the primary system QoS is maintained. Those channels that can not support the primary system QoS will be added into the channel set $\mathcal{V}$. With the current result of the interference violation test, for those channels belonging to $\mathcal{V}$, SFRA is not applicable. As a result, spectrum sensing is required. According to the spectrum sensing results, if the sub-channels in $\mathcal{V}$ are available, they can be removed from $\mathcal{V}$. At this moment, if $\mathcal{V}$ is empty, the interference violation test can be stopped since the primary systems QoS is maintained. Unfortunately, the sub-channels sometimes are detected unavailable and thus another interference violation test is required to update $\mathcal{V}$ and resource

allocation result according to the most recently obtained spectrum sensing results until $\mathcal{V} = \emptyset$. Then the optimal solution for resource allocation can be obtained. The algorithm for the proposed adaptive resource allocation scheme is given in Algorithm 2 as shown below. In this algorithm, the Algorithm 1 is applied to solve **P3** for each iteration.

Algorithm 2 Proposed resource allocation algorithm

Require:

$\mathcal{A} = \emptyset$, $\mathcal{N} = \{1, 2, ..., N\}$ for all the users;
${P_k}^{\max}$, $R^{\min}$, ${I_i}^{\max}$, violated channel set $\mathcal{V} = \emptyset$;

Ensure:

1. Solve **P3** with interference constraint for those channels belonging to $\mathcal{V}$ to get the corresponding power allocation $\mathbf{P}$ and channel allocation result $\rho_{i,k}$.
2. Update $\mathcal{V}$ according to interference violation test result. If $\mathcal{V} = \emptyset$, $\mathbf{P}^* = \mathbf{P}$ and $\rho^*_{i,k} = \rho_{i,k}$; else, corresponding SUs do spectrum sensing for the channels in $\mathcal{V}$. Update $\mathcal{A}$ and $\mathcal{N}$.
3. For each channel in $\mathcal{V}$, if it is available, remove it from $\mathcal{V}$. Update $\mathcal{V}$.

Until

$\mathcal{V} = \emptyset$, $\mathbf{P}^* = \mathbf{P}$, $\rho^*_{i,k} = \rho_{i,k}$.

Lastcon:

Optimal solution $\mathbf{P}^*$ and $\rho^*_{i,k}$;

Based on the optimal power and channel allocation results obtained here, those sub-channels that are able to support primary system QoS constitute the sub-channel groups for the corresponding SUs that operates the sensing-free strategy, SFRA. For the sub-channels that do violate the interference constraints in the iteration process of the proposed algorithm, the CBS has to perform spectrum sensing for these sub-channels and then include the results in the next iteration of power and channel allocation calculation as shown in Algorithm 2. The proposed algorithm avoids unnecessary spectrum sensing and hence reduces the energy consumption, at the price of more optimization computation of **P3**. This provides a tradeoff between sensing energy consumption and signal processing power consumption. When the number of channels is large, it is believed that the proposed algorithm is more promising.

3.6 Numerical Examples

In this section, we present simulation results to demonstrate the performance of the proposed resource allocation strategy and algorithms. We first consider the scenario shown in Fig. 3.1, where the secondary links attempt to access the spectrum of the primary system. Both the service radius of the primary system, R_1, and that of the CR system, R_2, are set to be 1000 m. The coordinates of CBS and PBS are $(0, 0)$ and $(-1500, 0)$, respectively. There are 5 SUs existing in this area with different x coordinates, and they have identical y coordinate of -200. We assume that the bandwidth of the primary system is 1.5 MHz, and is divided into 12 sub-channels, each having a bandwidth of 125 kHz. The total path-loss of each transceiver pair is assumed to be affected by both small-scale Rayleigh fading and large-scale path-loss, where the path-loss exponent r is 3. The probability of each sub-channel being unoccupied is 50%, the maximum transmission power of the SU $P^{\max}$ is 20 W, and the transmission power of the PBS P_p is 50 W. Unless stated otherwise, the minimum data rate requirement for each user is identical and ${R_k}^{\min}$ is 0.2 Mb/s, the noise power at CBS σ^2 and the QoS threshold of the primary system $I^{\max}$ are set to be -20 dBmW and -25 dBmW, respectively. All the results in this section for all the schemes are obtained under perfect spectrum sensing, and the case of imperfect sensing is out of the scope of this paper.

The SUs are located in different regions as shown in Fig. 3.1 and the distance between SUs located in Hybrid Region to a cell-edge PU can be calculated by $d_{SP}^{(k)} = D_k - R_1$, where D_k denotes the distance between the kth SU to the PBS. The results in the simulation are obtained by using a same set of random channel realizations for each value of $d_{SP}^{(k)}$. Fig. 3.2 shows the power consumption of SUs versus user ID with different resource allocation strategies when ${R_k}^{\min} = 0.2$ Mb/s. With the overlay-based scheme, only the channels being sensed idle are utilized. We do not give

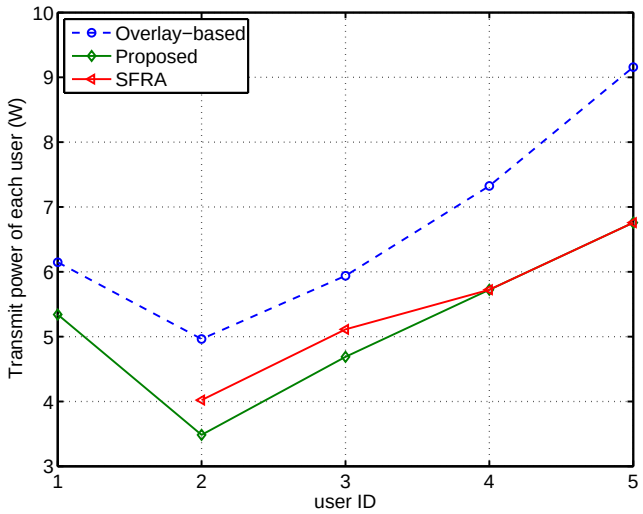

Figure 3.2: The transmit power of SUs versus user ID with different resource allocation strategies (x coordinates increase from -300 to 900).

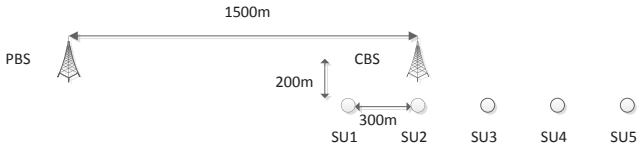

Figure 3.3: The location information for simulation.

the results with the underlay-based scheme since the resource allocation results using the underlay-based and the proposed scheme are identical for users in the Hybrid Region, which is the case in Fig. 3.3. The only difference lies in the power spent on spectrum sensing. The x coordinates of these SUs are set to increase from -300 to 900 with the distance of the adjacent SUs being 300 m as shown in Fig. 3.3. From the coordinates of the SUs, we know that all the SUs locate in the Hybrid Region. The corresponding channel allocation results with the proposed scheme are shown in Table 3.2. In this table we can see that SU 4 and SU 5 are assigned one more channel since they are relatively far away from the CBS compared to other SUs which leads to less channel gain due to the large scale fading. The number of iterations for executing Algorithm 2 is 3, and the interference violation test results are shown in Table 3.2. "YES" represents that the channel has ever been in the violated channel set $\mathcal{V}$. It

Table 3.2: Channel allocation results

	SU 1	SU 2	SU 3	SU 4	SU 5	violate
channel 1	0	0	0	0	1	NO
channel 2	0	1	0	0	0	YES
channel 3	0	0	0	1	0	NO
channel 4	0	1	0	0	0	YES
channel 5	0	0	0	0	1	NO
channel 6	0	0	1	0	0	YES
channel 7	1	0	0	0	0	YES
channel 8	0	0	0	1	0	NO
channel 9	1	0	0	0	0	YES
channel 10	0	0	0	1	0	NO
channel 11	0	0	0	0	1	NO
channel 12	0	0	1	0	0	NO

can be seen that spectrum sensing was performed for only 5 channels which means we saved 58% energy for spectrum sensing.

For the SUs being close to the worst-case PU ($d_{SP}^{(k)} = 217$ m), the interference constraints translate into very stringent transmit power constraints, so that SFRA provides no solution to guarantee the minimum data requirement as shown in Fig. 3.2. For the SU that is closest to the CBS ($d_{SP}^{(k)} = 513$ m), the consumed power curves for both the proposed scheme and overlay-based scheme decrease rapidly as a result of less path loss, attaining the minimum value around 3.5 W and 5 W, respectively. For the SUs located far away from the worst-case PU, the consumed power curves for all the schemes increase and we observe that the proposed approach is strictly superior to the overlay-based approach in terms of power consumption, and coincides with SFRA for the SUs which are sufficiently far from the worst-case PU.

Fig. 3.4 shows the energy efficiency of SUs versus user ID with different resource

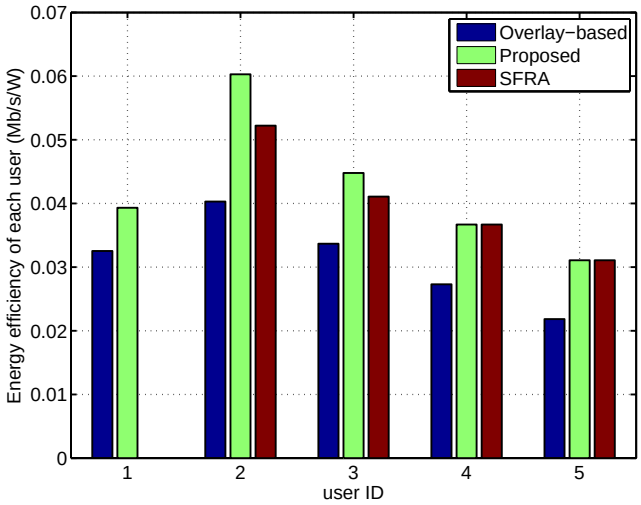

Figure 3.4: The energy efficiency of SUs versus user ID with different resource allocation strategies.

allocation strategy when ${R_k}^{\min} = 0.2$ Mb/s. We define energy efficiency for user k as

$$E^{(k)} = \frac{R_{act}^{(k)}}{\sum_{i \in \mathcal{A}^{(k)} \bigcup \mathcal{N}^{(k)}} P_{i,k}}, \tag{3.21}$$

where $R_{act}^{(k)}$ is the actual data rate based on a feasible power allocation solution. The equivalent metric for energy efficiency can be found in some publications, e.g., [31, 42, 45]. We notice that for the overlay/underlay-based approach, we have $R_{act}^{(k)} = R_k^{\min}$. However, for SFRA, which is based on the worst-case design, the actual achieved data rate $R_{act}^{(k)}$ is usually larger than the required data rate, i.e., $R_{act}^{(k)} > R_k^{\min}$. More specifically, when SFRA is applied, the resource allocation algorithm computes the achieved data rate using the second term in (3.1) which considers the interference from the PBS. However, such an interference does not exist if the spectrum resource is unoccupied by the primary system. Therefore, the actual achieved data rate in this case is a bit larger than the required data rate. From this figure, we can see that the proposed scheme outperforms the overlay-based scheme since more channel resources are utilized. When the SU is close to the CBS ($d_{SP}^{(k)} = 513$ m), the energy efficiency of

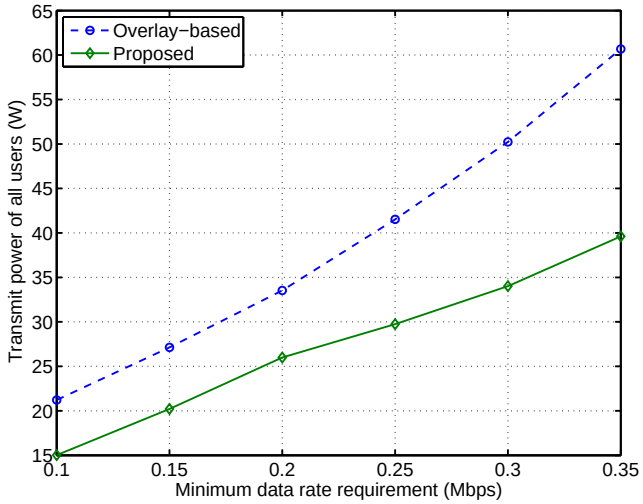

Figure 3.5: The transmit power of all SUs versus the minimum data rate requirement for each SU with different resource allocation strategies.

the proposed scheme is better than SFPA since the interference constraints of some channels are relaxed according to potential spectrum sensing results.

Fig. 3.5 shows the overall power consumption of all SUs with different resource allocation strategies, when the minimum data rate requirement ${R_k}^{\min}$ increases from 0.1 Mb/s to 0.35 Mb/s. In this figure, the performance curves of the proposed adaptive location-aware approach are compared with those of the overlay-based approach. The result of SFRA is not shown here since there is no solution for user 1 by applying SFRA. As can be observed from this figure, the overall transmit power for both the two schemes increase almost linearly as ${R_k}^{\min}$ increases. The proposed scheme has the best performance while the overlay-based approach consumes more power. This is because the proposed scheme sometimes utilize the subchannels which have large channel gain but detected as occupied channels in an overlay mode. The proposed scheme just utilizes these *good* channels subject to an interference constraint.

Since the SUs are moving, we change the x coordinates of these SUs to increase from -700 to 500. Now, by calculating D_k, we can find that user 1 is located in the Overlay Region and the other SUs locate in the Hybrid Region. For the SU located

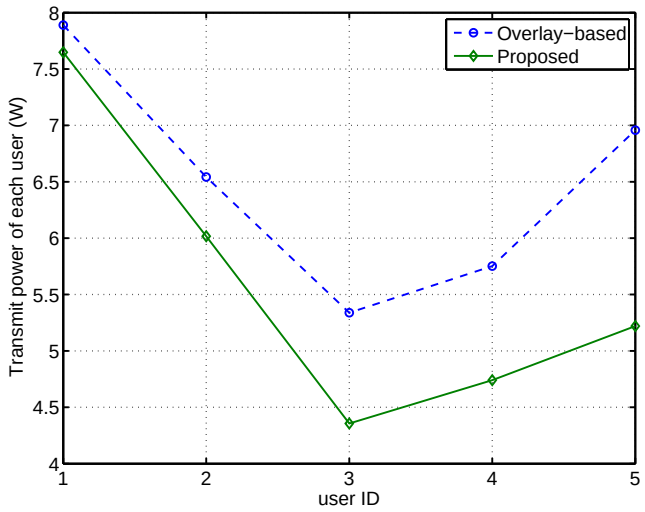

Figure 3.6: The transmit power of SUs versus user ID with different resource allocation strategies (x coordinates increase from -700 to 500).

in the Overlay Region, spectrum sensing has to be performed. Fig. 3.6 shows the power consumption of SUs for the Overlay-based scheme and the proposed scheme. The result of SFRA is not shown here since SFRA provides no solution due to SUs located close to PBS. From this figure, we can find that the power consumptions for both schemes are very close for those SUs located near the PBS. Although SU 1 is located in the Overlay Region, the proposed scheme still consumes less power since better channels are assigned to SU 1 with a more appropriate channel allocation. For the SUs located far away from the PBS, the proposed scheme consumes much less power compared to the overlay-based scheme.

To demonstrate the impact of geographical locations on energy efficiency, all the simulation results above are obtained by using a same set of random channel realizations for different users. We now consider instantaneous random channels for each SU to provide some detailed statistical insight into the simulations. Fig. 3.7 shows the probability density functions of energy efficiency for SU4 in Fig. 3.3 obtained by simulation of 1000 sets of channel realizations with different resource allocation schemes. The used simulation parameters are the same as those mentioned at the

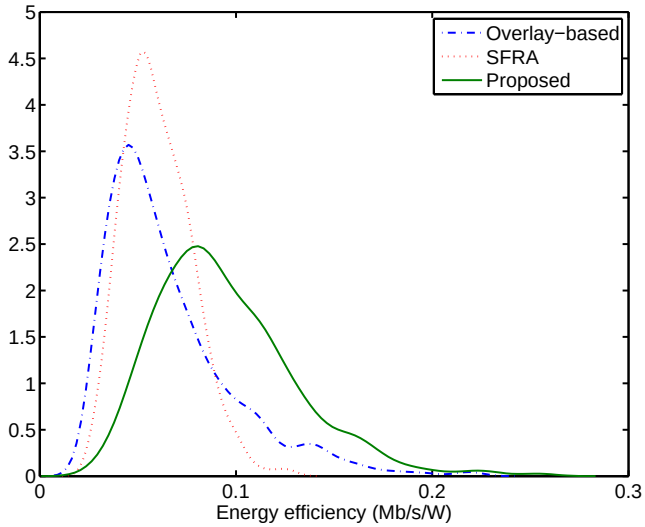

Figure 3.7: The probability density functions of energy efficiency with different resource allocation strategies.

beginning of this section except the channel information. Here we only give the result of SU4 since all the SUs have similar probability density functions and hence we take SU4 as an example.

From this figure, we can see that the mean value of energy efficiency with proposed scheme is around 0.07 Mbps/W while it is only about 0.03 for overlay and 0.05 for SFRA, respectively. Therefore, we can conclude that the SUs have the best performance by applying the proposed scheme. In summary, the proposed scheme is able to adapt to different resource allocation strategies for SUs located at different locations and achieves the maximal energy efficiency or minimal power consumptions in all scenarios.

3.7 Conclusions

This chapter has elaborated the role of adaptive resource allocation in CR networks in terms of energy efficiency since energy-efficiency oriented design is more and more important for wireless communications. Based on the existing research on resource

allocation for OFDM-based CR networks, this chapter proposes an adaptive hybrid resource allocation strategy to enhance the energy efficiency by utilizing spectrum and spatial opportunities. A novel adaptive power and channel allocation algorithm has been proposed to fulfill the proposed resource allocation strategy based on the interference violation test. In comparison between the existing scheme and the proposed resource allocation scheme, we have found that resource allocation by considering spatial information enhances the energy efficiency and avoids unnecessary spectrum sensing.

Chapter 4

Resource Allocation in Cognitive Radio Systems with Channel Uncertainty

In Chapters 2 and 3, we studied the resource allocation problem in CR systems for both the single user and multiple user case. The resource allocation optimization algorithm requires the channel state information (CSI) between CR transmitters and CR receivers or PUs. Among these CSIs, those for SU-to-CBS can be estimated by CBS. However, the CSI from SU to the hypothetical worst-case PU is difficult to acquire. First, there may not even exist a PU at the worst-case location. Second, usually the secondary network and the primary network have no explicit interaction. In this chapter, we examine the resource allocation problem with the unknown SU-to-PU channel information. The solution only utilizes the statistical behavior of the SU-to-PU channel, instead of the instantaneous CSI.

4.1 Introduction

As in conventional wireless systems, knowledge of the CSI is crucial for managing resource allocation. However, in a CR system, since it is not necessary for the PU system to exchange synchronization and channel training signals with SUs, the SU-to-PU channels are difficult to acquire accurately in practice. As a result, instead of the instantaneous channel information, the statistics of the SU-to-PU channels can be used instead when considering the interference caused by SU to PU in terms of average or probabilistic constraints [46]. The resource allocation and power control problem for CR systems with such channel uncertainty has been considered in, e.g., [46–49]. In [46], a cross-layer resource allocation scheme for underlay cognitive radio networks was formulated, in the presence of uncertain channel information from SU to PU. The authors of [47] considered the resource allocation problem for a cognitive radio base station communicating with multiple CR users in the downlink, and advocated a robust interference power constraint (guarantee tolerable interference to the PU system) to address channel uncertainty. Similarly, the authors of [48] proposed a robust distributed uplink power allocation algorithm for underlay cognitive radio networks with a view to maximizing the social utility of SUs when channel gains from SUs to PBS, and interference caused by PUs to the CBS are uncertain. In [49], power control was extended to the case where the channels between CR transceivers cannot be accurately acquired as well.

4.2 Motivation

As indicated in previous chapters, spectrum sensing is the primary technique employed by the CR system to detect the availability of licensed spectrum and protect the primary system from being harmfully interfered. However, spectrum sensing

schemes can only detect and localize active PU transmitters, but not inactive PU receivers, which may remain silent most of the time. Since localization of PUs based on the received signal strength (RSS) measurements over primary signalling messages is challenging for CR systems, the PU receiver locations must be assumed uncertain. This is the reason why we use a worst case design in the previous chapters (The PU receivers are assumed located at the boundary of the PU service region). As a result, the uncertainty in the PU receivers' locations indirectly generates uncertainty on the propagation gains of the SU-to-PU channels.

Channel estimation in CR systems is challenging, since the SUs gain access to the medium only intermittently, and the incumbent PU system often does not explicitly support channel estimation for CR systems. In addition, SUs may not have prior knowledge of PU signal characteristics, and thus are forced to resort to less efficient channel estimation techniques. Nevertheless, PU transmissions must be strictly protected from the interference due to SUs. Therefore, it is widely recognized that resource allocation for SUs must account for channel uncertainty.

Therefore, in this chapter, we solve the resource allocation problem in CR systems with channel uncertainty. Typically, uncertainty in the parameters of an optimization problem is captured either deterministically or statistically. Under the deterministic approach, bounded uncertainty sets of the parameters should be assumed while the parameters are viewed as random for the statistical approach, and chance constraints will be constructed from the distributions of the parameters. In this work, we focus on the chance constraint approach to derive the optimal resource allocation for CR systems.

4.3 Problem Formulation

Consider the same scenario as in Chapter 3, that one CR system coexists with one primary system, where K mobile SUs communicate with the cognitive base station (CBS) in the uplink and the corresponding worst-case PUs receive signals from the primary base station (PBS), as depicted in Fig. 3.1.

The QoS problem for different cognitive power allocation strategies can be formulated by a general framework same as in Chapter 3 except the interference constraint:

$$
\begin{aligned}
&(\mathbf{P4.1}) \quad \min_{P_{i,k},\rho_{i,k}\forall i,k} \ \textstyle\sum_{k=1}^{K}\sum_{i\in\mathcal{A}\bigcup\mathcal{N}}\rho_{i,k}P_{i,k} \\
&\text{s.t. } R_k = \sum_{i\in\mathcal{A}}\rho_{i,k}\mathcal{C}\left(\frac{P_{i,k}h_{i,k}^{SS}}{\sigma^2}\right) \\
&+\alpha^{(k)}\sum_{i\in\mathcal{N}}\rho_{i,k}\mathcal{C}\left(\frac{P_{i,k}h_{i,k}^{SS}}{\sigma^2+P_p h_i^{PS}}\right) \geq R^{\min}, \forall k && (4.1) \\
&\textstyle\sum_{i\in\mathcal{A}\bigcup\mathcal{N}}\rho_{i,k}P_{i,k} \leq {P_k}^{\max}, \forall k && (4.2) \\
&\alpha^{(k)}\rho_{i,k}\Pr\{P_{i,k}L_{i,k}^{SP}h_{i,k}^{SP} > I_i^{\max}\} \leq \epsilon, \qquad \forall i\in\mathcal{N}, \forall k, && (4.3) \\
&\sum_{k=1}^{K}\rho_{i,k} \leq 1, \rho_{i,k}\in\{0,1\}, \forall k, i, && (4.4)
\end{aligned}
$$

where most of the parameters are explained in Chapter 3, and $h_{i,k}^{SP}$ denotes the channel gain from the k-th SU to the worst case PU on channel i. The constraint (4.3) enforces the interference to the PU exceed $I_i^{\max}$ with probability at no larger than ϵ. Unlike the channels between SU transceivers, it is difficult to estimate $h_{i,k}^{SP}$ precisely, due to the lack of cooperation from the PU system.

4.3.1 Random channel state information with finite support

If we assume $h_{i,k}^{SP}$ to be random and independent with arbitrary probability distribution, the mean value is $\overline{h}_{i,k}^{SP}$ and $h_{i,k}^{SP} - \overline{h}_{i,k}^{SP}$ varies in segments $[-\hat{h}_{i,k}^{SP}, \hat{h}_{i,k}^{SP}]$. Then

according to [47] the approximation of (4.3) can be given as

$$\alpha^{(k)}\rho_{i,k}P_{i,k}L_{i,k}^{SP}\big(\overline{h}_{i,k}^{SP}+\sqrt{2\log(\frac{1}{\epsilon})}\hat{h}_{i,k}^{SP}\big)\leq I_i^{\max} \tag{4.5}$$

To solve **P4.1**, we just need to substitute the channel gain in (4.5) into (3.16), then run Algorithm 1 in Chapter 3.

4.3.2 Gaussian random channel state information

If we assume $h_{i,k}^{SP}$ to be Gaussian random with mean value $\overline{h}_{i,k}^{SP}$ and unit variance, the interference constraint (4.3) can be written as [47]

$$\alpha^{(k)}\rho_{i,k}\big(\frac{I_i^{\max}}{P_{i,k}L_{i,k}^{SP}}-\overline{h}_{i,k}^{SP}\big)\geq Q^{-1}(\epsilon), \tag{4.6}$$

where $Q(\cdot)$ is the standard Gaussian tail function. Then substitute the terms in (4.6) into (3.16) and run Algorithm 1 in Chapter 3, we can get the optimal solution.

4.4 Numerical Examples

In this section, we present simulation results to demonstrate the performance of the system with channel uncertainty. The scenario we considered is the same as in Chapter 3, as well as all the parameter settings.

If we assume $h_{i,k}^{SP}$ to be random with mean value $\overline{h}_{i,k}^{SP}$ and $h_{i,k}^{SP}-\overline{h}_{i,k}^{SP}$ varying in segments $[-\hat{h}_{i,k}^{SP},\hat{h}_{i,k}^{SP}]$. Then (4.5) will be adopted as constraint. In this simulation, we set $\overline{h}_{i,k}^{SP}$ to 1 and $\hat{h}_{i,k}^{SP}$ to 0.5.

Fig. 4.1 shows the sensitivity of the system performance to the PU interference constraint. The transmit power of each SU is plotted against user ID for different resource allocation strategies. In this section, we are interested in the effect of ϵ.

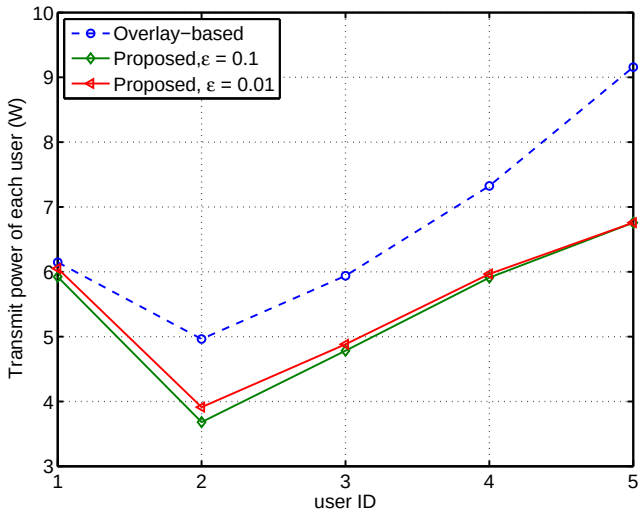

Figure 4.1: The transmit power of SUs versus user ID with different resource allocation strategies (x coordinates increase from -300 to 900).

From this figure, we can see that transmit power of each SU is larger when $\epsilon = 0.01$ except for SU 5. This is because the interference constraint is tight when $\epsilon = 0.01$, one user can not allocate too much power on the channels with large propagation gains. Instead, some more power is allocated on the channels with smaller propagation gains. Thus, more transmit power is required to achieve the minimum data requirement. Since SU 5 is located far away from the PU service region, the sensitivity of the system performance to the PU interference constraint can be neglected, thus we can see that there is not much difference between the cases with $\epsilon = 0.1$ and $\epsilon = 0.01$.

Fig. 4.2 depicts the transmit power for SU 4 with overlay-based scheme and the proposed scheme. The values of ϵ were varied. It can be verified that the required transmit power decreases as ϵ grows larger, as this amounts to more lenient interference constraints. Less transmit power means larger energy efficiency, but it leads to larger probability on violating the interference constraint.

If we assume $h_{i,k}^{SP}$ to be Gaussian random with mean value $\overline{h}_{i,k}^{SP} = 1$ and unit variance, then (4.6) will be adopted as constraint.

Fig. 4.3 shows the sensitivity of the system performance to the PU interference

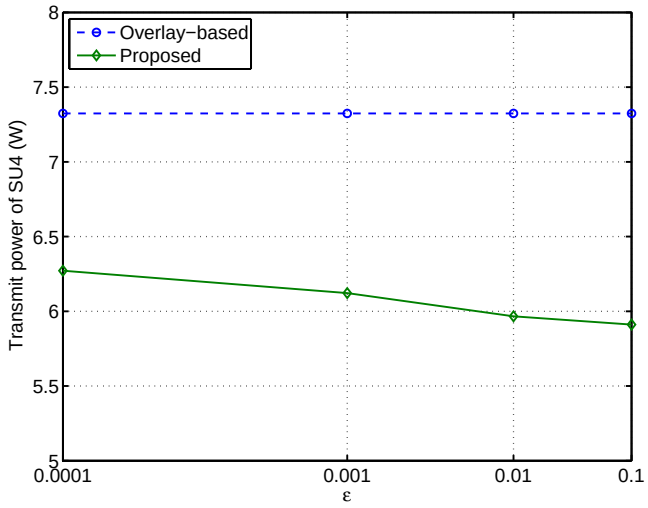

Figure 4.2: The transmit power of SU4 versus ϵ with different resource allocation strategies.

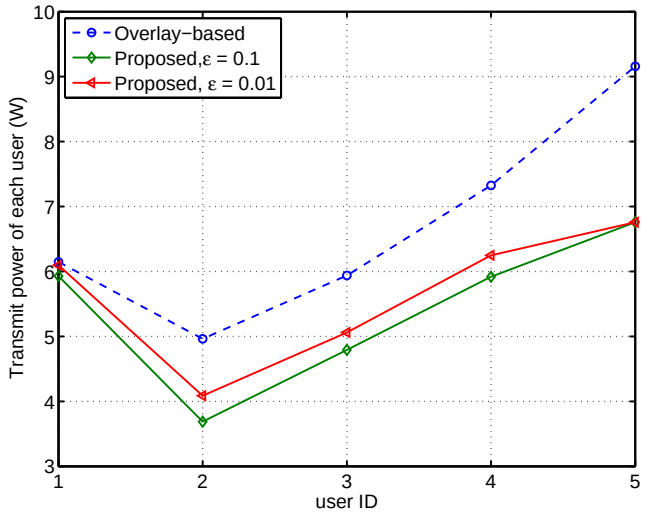

Figure 4.3: The transmit power of SUs versus user ID with different resource allocation strategies (x coordinates increase from -300 to 900, SU-to-PU channel is assumed to be Gaussian random).

constraint when SU-to-PU channel is assumed to be Gaussian random with mean value $\overline{h}_{i,k}^{SP} = 1$ and unit variance. The transmit power of each SU is plotted against user ID for different resource allocation strategies. The trend of the curves in Fig. 4.3 is similar with that of Fig. 4.1, but the gap of the two curves for $\epsilon = 0.1$ and $\epsilon = 0.01$ in this figure is larger that that of Fig. 4.1. This means that the probability

constraint ϵ has greater impact on the system performance when the uncertain channel is assumed to be Gaussian random.

4.5 Conclusion

A power consumption minimization problem was formulated for a CR system employing OFDMA in this chapter. Due to the uncertainty present in the CR-to-PU channel, a robust interference constraint with channel uncertainty was imposed to protect the PU system. For different assumptions on the uncertain channel, we show two optimization approaches to handle this problem. Numerical tests have verified the efficiency of the proposed scheme and demonstrated that the CR system can achieve a better energy efficiency at the price of generating harmful interference to PU system with higher probability.

Chapter 5

Multiple Access and Data Reconstruction in Wireless Sensor Networks based on Compressed Sensing

5.1 Introduction

Introduced as a technique for finding sparse solutions to underdetermined linear systems, compressed sensing (CS) has now found widespread applications in both signal processing and communication communities, ranging from data compression [50], data acquisition [51], inverse problems [9], and channel coding [52]. An essential idea of CS is to explore the fact that most natural phenomena are sparse or compressible in some appropriate basis. By acquiring a relatively small number of samples in the "sparse" domain, the signal of interest can be reconstructed with high accuracy through well-developed optimization procedures [12, 13, 51]. Recently, this technique has been proposed to achieve energy-efficient multiple access [53–58] or routing pro-

tocol design [59] for wireless networks. In the case of medium access control (MAC), by considering the scenario that only a small portion of transmitters are active at a certain time instant, the aggregated signal from all the transmitters can be viewed as a sparse signal in the dictionary of an identity matrix. It has been demonstrated that CS-based MAC schemes have advantages ranging from increased power efficiency [53], enhanced throughput [54], as well as improved identity detection [55–57].

In a wireless sensor network (WSN), usually the readings of the sensor nodes have both spatial correlation (due to the closeness of sensors' geographical locations) and temporal correlation (due to the smooth variations of the real world signal). These redundancies indicate that sensor data is compressible along these dimensions. Thus, CS-based design can recover the whole network data from a few active sensor nodes, which effectively reduces the overall number of transmissions from the sensor nodes and saves network power. In fact, energy-efficient design for WSNs is a very important topic that has been addressed by many existing works [14–16, 60–64]. In [14, 15], the authors propose improved contention-based MAC protocols to save energy for WSNs by periodic listen and sleep as well as collision avoidance. In [16, 60, 61], cross-layer designs are proposed to optimize energy consumption in WSNs based on time division multiple access (TDMA). Multiple-input and multiple-output (MIMO) and cooperative MIMO techniques are adopted to enhance the spectral efficiency and achieve energy saving for WSNs in [62,63]. Besides, a likelihood-based multiple access strategy has been proposed in [64] for parameter estimation in energy-constrained WSNs. As we shall show, CS-based scheme is also an energy-efficient scheme for medium access control in WSNs.

The first part of this chapter complements our previous work [58] by providing an in-depth analysis of CS-based multiple access schemes from a physical layer perspective. To the best our knowledge, we make the first attempt in studying the impact

of communication signal-to-noise ratio (SNR) on the reconstruction performance of CS-based MAC schemes, which has not been considered by the existing literature. The main contributions are summarized as follows.

- The complete CS-based symbol recovery process in a multiple access channel has been described. In particular, reconstruction/detection with respect to modulated symbols in the physical layer rather than higher layer sensor measurement has been emphasized, which enables us to investigate the impact of SNR on the accuracy of the CS-based transmission symbol recovery. We prove that the l_2 norm upper bound of the reconstruction error decreases as $\mathcal{O}(\mathsf{SNR}^{-1})$ (cf. Property 1).

- Multiple antennas are equipped at the receiver to increase the number of random projections observed by the receiver. In the existing CS-based MAC work, the sensor nodes have to retransmit their data if the number of observations is not sufficient for successful CS recovery. With multiple antennas at the receiver, the times of data retransmission can be reduced significantly.

- The decision problem of distinguishing between active and inactive transmitters after symbol recovery has been identified. Due to the reconstruction error introduced in the recovery process, the receiver can incorrectly detect an inactive transmitter to be active, especially when the communication SNR is low. To tackle this problem, a novel decision boundary for the exemplary quadrature phase-shift keying (QPSK) modulated signal[1] has been proposed, the effectiveness of which has been validated through simulations.

[1]We note that QPSK has been adopted in the physical layer specifications of IEEE standard 802.15.4 and is selected here as an example to demonstrate how the proposed design works under a practical modulation scheme. The design methodology in this study can be applied to study other modulation schemes as well.

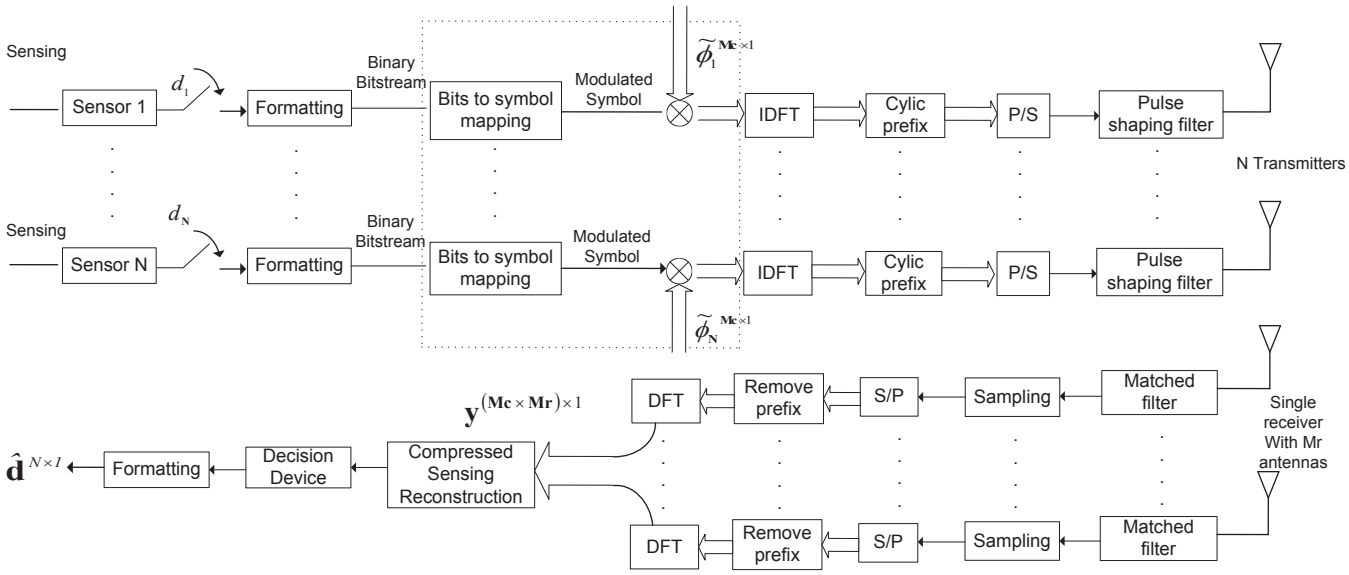

Figure 5.1: Transmitter and receiver structure.

- A detailed performance comparison between carrier sense multiple access (CSMA) and the proposed CS-based MAC has been performed. In particular, it is found that 1) the system SNR affects positively the throughput performance of both CSMA and CS-based MAC schemes. The impact, however, is much more salient on the CS-based scheme (cf. Fig. 5.10) and 2) CSMA reaches a maximum achievable throughput limit as the number of concurrent transmissions increases. In contrast, the CS-based MAC scheme accommodates concurrent transmissions well as long as the number of observations are sufficiently large.

Having investigated the applicability of compressed sensing in random medium access, the second part of this chapter deals with data recovery for the whole network over a certain time period. For instance, the authors in [53] propose a random access scheme where each sensor is activated for transmission based on an access probability. By simply discarding the colliding data packets from concurrent medium access, the receiver can still recover all the data of interest based on the successfully received data packets using compressed sensing. The authors in [65] propose a distributed matched

source-channel communication scheme applying compressed sensing theory for estimation of sensed data at the fusion center, which is also based on spatially correlated data measurements in wireless sensor networks. By exploiting temporal correlation between the signal components, the authors in [66] propose a belief propagation-based CS algorithm to enhance data reconstruction performance at the receiver.

Rather than utilizing sparsity in one single domain, as in the aforementioned works, we propose a CS-based network data recovery scheme utilizing both spatial and temporal correlation in a joint manner. To be specific, at one time instant, the fusion center of the wireless sensor network receives data packets from the active sensor nodes simultaneously and recovers the spatially compressible readings of all the sensor nodes in the network. In the event of network data recovery failure due to insufficient number of observations in the spatial domain, the fusion center could restore some of the un-recovered inactive sensor readings by CS recovery in the temporal domain if there are sufficient number of observations (obtained by active sensor data transmission and spatial domain recovery) for these sensors. Hence, by successively applying compressed sensing in communication and network data recovery, the proposed scheme incorporates all the benefits from existing schemes and achieves data measurement collection and reconstruction in the most energy-efficient manner.

The remainder of the chapter is organized as follows. In Section 5.2, system model is described and Section 5.3 discusses CS symbol recovery for multiple access in wireless communication. In Section 5.4, compressed sensing for network data recovery is described. In Section 5.5, several numerical examples are provided to illustrate the performance enhancement of the proposed scheme over traditional multiple access schemes. Finally, conclusions are drawn in Section 5.6.

5.2 System Model

Consider a wireless sensor network consisting of $\mathcal{N} = \{1, 2, ..., N\}$ sensor nodes deployed to sense certain natural phenomenon. The sensors report their data measurements to a single receiver (e.g., fusion center) with M_r antennas, each of which has M_c degree of freedom. Here, the degree of freedom M_c indicates the dimension of one antenna's received signal vector, which represents the number of channels available in either time or frequency domain. We assume that channel knowledge is available at the receiver side (CSIR) and without loss of generality, quadrature phase-shift keying (QPSK) is applied for digital modulation in this paper. Fig. 5.1 illustrates the CS-based communication system model assuming the M_c degree of freedom is achieved by frequency subchannels and hence orthogonal frequency division multiplexing (OFDM) is used as an example.

5.2.1 Traffic Model

The sensor nodes report to the destination receiver periodically. The duration of one reporting period T_f, which we refer to as one time frame, is assumed to be less than the coherence time of the natural phenomenon. This assumption ensures that the monitored environment remains static in one time frame, implying that data measurements only need to be delivered to the receiver once during one entire frame. The sensors are referred to as being *active* when they are engaged in data transmission in one time frame. Due to temporal and spatial correlations in the sensor readings and to conserve power of the sensor nodes, only a small number of active sensor nodes, denoted by r, are required to transmit during one time frame. To achieve this, a reasonable modeling approach, or implementation technique, is to equip each sensor with a Bernoulli random generator with success probability λ

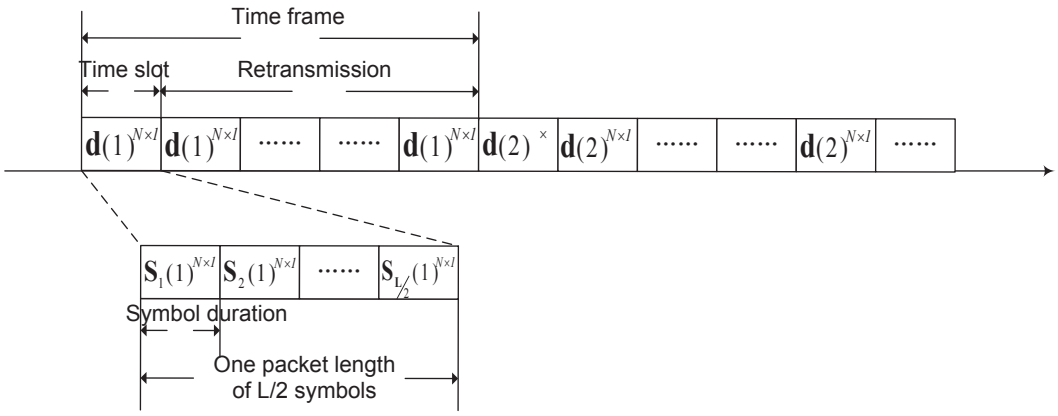

Figure 5.2: Sensor data and modulated symbol frame structure (without sensing vector weighting).

satisfying $\lambda N \ll N$ [53]. Hence, the total number of active sensors in one time frame follows a Binomial distribution with parameters N and λ, i.e., $r \sim B(N, \lambda)$. At the beginning of each time frame, each generator performs one independent Bernoulli trial, the outcome of which indicates whether sensor node i will transmit its data measurement d_i to the receiver in this time frame. By designing λ to be sufficiently small, the data from the few active sensor nodes can be recovered at the receiver through compressed sensing. Besides, we denote the set of active sensor nodes in one time frame as $\mathcal{A} = \{a_1, ..., a_r\}$. The data vector from all the sensor nodes is denoted as $\mathbf{d} = [d_1, \cdots, d_N]^T$ and the data vector from only the active sensor nodes as $\mathbf{d}_{\mathcal{A}} = [d_{a_1} \cdots d_{a_r}]^T$.

A key issue here is to determine a proper value for the access probability λ, the value of which affects both the feasibility and effectiveness of network data recovery based on spatial correlations. Let us denote the spatial sparsity of the sensor readings as r_s. According to [67], the required number of observations m_s for successful network data recovery based on spatial correlations can be obtained as $m_s = O(r_s \log N)$[2]. To satisfy this requirement, we select the access probability $\lambda = m_s/N$, which ensures

[2]Throughout the chapter, the logarithm operator log denotes the natural logarithm.

that the required number of observations is guaranteed on an average sense. To be specific, given that the number of active sensor nodes r follows a Binomial distribution $r \sim B(N, \lambda)$, the mean value of the number of active sensors r can be calculated as $\mathbb{E}(r) = \lambda N = m_s$, where $\mathbb{E}(\cdot)$ is the expectation operator.

Prior to transmitting, the data of the active sensor nodes must be converted to binary digits and packets for digital transmission. We assume that each time frame T_f is divided into I time slots, the length of which is defined as the time for each sensor to transmit one data packet. Without loss of generality, we assume that the data packets from all the sensor nodes are of the same length, denoted as L bits. Hence, for a given transmission data rate R, the number of time slots in one time frame, denoted by I, or equivalently, the maximum number of data packets that can be successfully transmitted to the receiver, is given by $I = RT_f/L$. Fig. 5.2 illustrates the frame and data packet structures. Given that the data packet is of L-length bits and QPSK is used, each active sensor will transmit $L/2$ symbols during one time slot. At the beginning of one time frame, the active sensors transmit simultaneously in the first time slot and the receiver obtains $M_c \times M_r$ observations according to the signal model (5.2) in the next section. These active sensor nodes shall keep on transmitting the same packets in the subsequent time slots, until sufficient number of observations has been collected at the receiver. The stopping rule shall be explained in Section 5.3. We note that since most of the sensor nodes are inactive, the transmitted data $\mathbf{d}(l)$ of the l-th time frame is sparse, implying that modulated symbol vectors in Fig. 5.2 are sparse as well. We then move on discussing the signal model.

5.2.2 Signal Model

The signal transmission process is illustrated by considering QPSK-modulated symbols as shown in Fig. 5.1. The M_c degree of freedom of the wireless channel represents

the number of subcarriers for OFDM[3]. Observe in Fig. 5.1 that the sensor readings are firstly converted to binary bit streams via formatting and then converted to modulation symbols via constellation mapping.

In time slot n during one time frame, a sensing matrix $\hat{\mathbf{\Phi}}(n) = [\widetilde{\boldsymbol{\phi}}_1(n) \cdots \widetilde{\boldsymbol{\phi}}_N(n)]$ is selected randomly from an orthonormal basis $\mathbf{\Phi} \in \mathbb{R}^{N \times N}$, where $\widetilde{\boldsymbol{\phi}}_i(n) \in \mathbb{C}^{M_c \times 1}$ is referred to as the sensing vector for sensor node i and the entries are independently identically distributed (i.i.d.) realizations of zero-mean random variables. Next, within each symbol duration of time slot n, active sensor node i has the modulated symbol s_i to be sent to the receiver. By multiplying s_i with its corresponding sensing vector $\widetilde{\boldsymbol{\phi}}_i(n)$, all the active sensor nodes transmit the resulting symbols to the single receiver simultaneously, as illustrated in Fig. 5.1.

After down conversion and matched filtering at the receiver, within each symbol duration, the observed signal at each antenna of receiver is the summation of the normalized QPSK symbol $s_i = \pm\frac{\sqrt{2}}{2} \pm \frac{\sqrt{2}}{2}j$ multiplied by the sensing vector $\widetilde{\boldsymbol{\phi}}_i(n)$ of the active sensor node $i \in \mathcal{A}$. Assuming perfect synchronization and identical transmit power of each sensor node on different M_c subchannels, the received signal vector at the kth antenna can be written as

$$\begin{aligned} \mathbf{y}^k(n) &= \sum_{i \in \mathcal{A}} \left(\sqrt{P_i} s_i \widetilde{\boldsymbol{\phi}}_i(n)\right) \circ \mathbf{h}_i^k(n) + \mathbf{w}^k(n) \\ &= \sum_{i=1}^{N} \left(x_i \widetilde{\boldsymbol{\phi}}_i(n)\right) \circ \mathbf{h}_i^k(n) + \mathbf{w}^k(n), \end{aligned} \tag{5.1}$$

where the operator $\circ$ denotes the Hadamard product, $\mathbf{h}_i^k(n) \in \mathbb{C}^{M_c \times 1}$ the channel vector (across all the frequency bands) from sensor node i to the kth antenna of the receiver, the entries of which are complex Gaussian random variables with zero mean

[3]Being different from the conventional OFDM, for each sensor, the transmitted data over all the subcarriers are an identical information symbol weighted by a random sensing vector.

and unit variance, $\mathbf{w}^k(n) \in \mathbb{C}^{M_c \times 1}$ the measurement noise, and $x_i = \sqrt{P_i} s_i \mathbb{1}_{i \in \mathcal{A}}$ the product of the transmit power and the transmitted symbol of the active sensor node i, where the notation $\mathbb{1}_{i \in \mathcal{A}}$ equals 1 for $i \in \mathcal{A}$ and 0 otherwise.

Then the received signal at the receiver is given by

$$\mathbf{y}(n) = \big(\hat{\mathbf{\Phi}}'(n) \circ \mathbf{H}(n)\big)\mathbf{x} + \mathbf{w}(n), \tag{5.2}$$

where $\mathbf{y}(n) = [\mathbf{y}^1(n)^T \cdots \mathbf{y}^{M_r}(n)^T]^T$, $\hat{\mathbf{\Phi}}'(n) = [\underbrace{\hat{\mathbf{\Phi}}(n)^T \cdots \hat{\mathbf{\Phi}}(n)^T}_{M_r}]^T \in \mathbb{C}^{(M_c \times M_r) \times N}$, $\mathbf{x} = [x_1 \cdots x_N]^T$ and $\mathbf{H}(n) = \begin{bmatrix} \mathbf{h}_1^1(n) & \cdots & \mathbf{h}_N^1(n) \\ \vdots & \vdots & \vdots \\ \mathbf{h}_1^{M_r}(n) & \cdots & \mathbf{h}_N^{M_r}(n) \end{bmatrix}$.

Observe from (5.2) that the receiver obtains $M_c \times M_r$ observations during one symbol duration. If the number of observations is not sufficient for CS recovery, retransmission is required. Keep retransmitting the same packet till the end of the p-th time slot, the received signal can be written as

$$\mathbf{z} = \mathbf{\Psi}\mathbf{x} + \mathbf{W}, \tag{5.3}$$

where the received signal $\mathbf{z} = [\mathbf{y}^T(1) \cdots \mathbf{y}^T(p)]^T$, the sensing matrix $\mathbf{\Psi} = [\big(\hat{\mathbf{\Phi}}'(1) \circ \mathbf{H}(1)\big)^T \cdots \big(\hat{\mathbf{\Phi}}'(p) \circ \mathbf{H}(p)\big)^T]^T$, and the noise $\mathbf{W} = [\mathbf{w}^T(1) \cdots \mathbf{w}^T(p)]^T$.

5.3 Compressed Sensing Symbol Recovery for Multiple Access in Wireless Communication

In this section, we describe the CS-based communication system in detail and discuss the sensing matrix of our model.

5.3.1 CS-Based Symbol Reconstruction

As illustrated by Fig. 5.1, for each antenna at the receiver, the received signal goes through a matched filter and the received signals via all the antennas become the input of compressed sensing reconstruction algorithm after sampling process. During certain time frame, by the end of the p-th time slot, the receiver obtains $p \times M_c \times M_r$ observations of the sparse modulated symbols, which can be recovered by solving the following l_1 minimization problem

$$\begin{aligned} \mathbf{P1} \quad & \underset{\mathbf{x}}{\text{minimize}} \quad \|\mathbf{x}\|_1 \\ & \text{subject to} \quad \|\mathbf{z} - \mathbf{\Psi}\mathbf{x}\|_2 \leq \varepsilon, \end{aligned} \tag{5.4}$$

where ε is a bound of the amount of noise in the data. Problem **P1** belongs to the class of basis pursuit (BP) problems [68], which admits efficient problem-solving algorithms such as the least absolute shrinkage and selection operator (LASSO) algorithm or the MATLAB toolbox l_1-Magic [69][4]. Note that as the number of observations at the receiver increases with time, the dimensions of both $\mathbf{z}$ and $\mathbf{\Psi}$ in (5.4) increase, as well as the symbol recovery accuracy. Thus, by tracking the difference of the reconstructed symbol vectors between two consecutive time slots, the active sensor nodes can be informed to stop transmission when the difference is less than a pre-defined threshold η. Otherwise, the sensor nodes will keep on transmitting till the end of this frame. A number of points worth mentioning are as follows.

- As in [53], the number of observations required for accurate symbol recovery can be estimated, which is around $4r$ in our case. To reduce the overhead of receiver-side signal processing, the receiver is set to start performing symbol

[4]Note that the proposed MAC approach can work with any CS-based reconstruction algorithm. The toolbox l_1-Magic has been adopted as an example to demonstrate the effectiveness of the proposed approach.

recovery (i.e., solving (5.4)) from time slot $\alpha = \lfloor \frac{3m_s}{M_c \times M_r} \rfloor$, where m_s equals the mean value of the signal sparsity r.

- What goes through the CS-based symbol recovery procedure is the modulation symbol $\mathbf{x}$ rather than the actual raw data $\mathbf{d}$. The raw data $\mathbf{d}$ is converted to a packet of L bits which are then modulated into $L/2$ QPSK symbols for physical layer transmission. Given that the number of active sensor nodes in time slot n satisfies $r \ll N$, we know that $\mathbf{x}$ is sparse in the dictionary of an identity matrix.

- The output of the CS-based symbol recovery (5.4) is $\hat{\mathbf{x}}$, through which the transmitted channel fading (c.f. the definition of $\hat{\mathbf{x}}$ ensuing (5.5) and (5.2), respectively.).

- A total of $L/2$ symbols are transmitted during one time slot from each active sensor node, which implies that CS-based symbol recovery will perform $L/2$ times during one time slot if the receiver has started to perform CS recovery.

- The identity information does not need to be sent with the data packets, since such information can be identified from the recovered symbols (based on the positions of the non-zero elements).

- The capacity of the proposed method in one time frame can be treated as the maximum allowable number of active sensors r in this time frame, multiplied by the effective data rate L/T_f, i.e., $C = Lr/T_f$. Note that in order for CS to apply, the number of active sensors r should be much smaller than the total number of sensors N. Then, for a WSN with M_c sub-channels and M_r antennas at the receiver, the maximum number of collectable observations satisfies $m \leq IM_cM_r$, where I is the number of time slots in one time frame calculated in Section

5.2.1. Finally, based on the relationship between the required the number of observations m and the sparsity r, which is $m = O(r \log N)$ [67], the capacity of the proposed method can be expressed as $C = O(RM_cM_r/\log N)$.

Finally, the reconstructed symbols of all sensors are detected by a decision device into binary bits (cf. Section 5.3.4). Note that the decision device will distinguish between active and inactive sensors. Once all the bits in a packet for each active sensor are obtained, they are formatted back to the decimal data of that sensor. This way the fusion center obtains all the active sensor data.

5.3.2 Discussions on Sensing Matrix Selection

Observe from (5.3) that the *actual* sensing matrix utilized in the symbol recovery process $\mathbf{\Psi}$ comprises of the Hadamard products $\hat{\mathbf{\Phi}}'(n) \circ \mathbf{H}(n)$ $(n = 1, ..., p)$, rather than the matrix $\hat{\mathbf{\Phi}}'(n)$[5]. This implies that in principle, the matrix $\hat{\mathbf{\Phi}}'(n)$ should be appropriately chosen such that the sensing matrix $\mathbf{\Psi}$ achieves minimum coherence with the dictionary in which the intended signal is sparse. To this end, we discuss three special cases on sensing matrix selection.

Case 1: Under slow and frequency-flat fading, the channel remains static during one time frame and is identical across different subchannels for each sensor node. When the receiver has only single antenna ($M_r = 1$), the received signal can be equivalently rewritten as

$$\mathbf{z} = [\hat{\mathbf{\Phi}}'(1)^T \cdots \hat{\mathbf{\Phi}}'(p)^T]^T \mathbf{x} + \mathbf{W}, \tag{5.5}$$

[5]Note that for the ease of theoretical derivation, the sensing matrix is usually assumed to be selected from an orthonormal basis. Nevertheless, such a restriction is not an essential requirement [13].

where $\mathbf{x} = [x_1 \cdots x_N]^T$ with $x_i = \sqrt{P_i} h_i s_i \mathbb{1}_{i \in \mathcal{A}}$ where the channel h_i is combined with data symbol s_i. Thus, the actual sensing matrix for CS recovery becomes the matrix $[\hat{\mathbf{\Phi}}'(1)^T \cdots \hat{\mathbf{\Phi}}'(p)^T]^T$.

Case 2: The channel remains static during one time frame but is independent across different subchannels and different antennas for each sensor node. In this case, $\mathbf{H}(n) = \mathbf{H}, (n = 1, ..., p)$ and the received signal can be rewritten as

$$\mathbf{z} = [\left(\hat{\mathbf{\Phi}}'(1) \circ \mathbf{H}\right)^T \cdots \left(\hat{\mathbf{\Phi}}'(p) \circ \mathbf{H}\right)^T]^T \mathbf{x} + \mathbf{W}, \tag{5.6}$$

where $\mathbf{H}$ is a random channel matrix with independent complex Gaussian random variables as elements. Thus, $\hat{\mathbf{\Phi}}'(n)$ makes the observations different over time.

Case 3: When the channel coefficients over M_c subcarriers, M_t antennas and multiple time slots are random and independent, the channel matrix $\mathbf{H}(n)$ alone can be used as the sensing matrix, thereby eliminating the necessity of sensing matrix $\hat{\mathbf{\Phi}}$ design. Then, the received signal can be written as

$$\mathbf{z} = [\mathbf{H}^T(1) \cdots \mathbf{H}^T(p)]^T \mathbf{x} + \mathbf{W}, \tag{5.7}$$

where the channel $[\mathbf{H}^T(1) \cdots \mathbf{H}^T(p)]^T$ becomes the actual sensing matrix for CS recovery. Note that in this case, the coherence between the sensing matrix (i.e., the channel) and the dictionary is beyond the control of the system designer. Nevertheless, we shall demonstrate that as long as the channel is fast-varying and independent over different subchannels and antennas, satisfactory reconstruction performance can be achieved.

5.3.3 Robustness of CS Reconstruction

The robustness of the current CS theory relies heavily on a notion called restricted isometry property (RIP) which was first introduced in [70]. To facilitate the proof of RIP of the sensing matrices, we introduce the definition of isometry constant [13].

Definition 2. For each integer $r = 1, 2, ...$, define the isometry constant δ_r of a matrix $\mathbf{\Psi}$ as the smallest number such that

$$(1 - \delta_r)\|\mathbf{x}\|_2^2 \leq \|\mathbf{\Psi}\mathbf{x}\|_2^2 \leq (1 + \delta_r)\|\mathbf{x}\|_2^2 \tag{5.8}$$

hold for all r-sparse vectors $\mathbf{x}$.

The matrix $\mathbf{\Psi}$ is said to loosely obey the RIP of order r if δ_r is not too close to one. In order to ensure the success and robustness of CS, the sensing matrix should satisfy the RIP [10, 11, 71–73]. Next, we prove that all the sensing matrices of the three cases discussed above satisfy the RIP.

It has been established in [72] that a random matrix with N columns, whose entries are i.i.d. realizations of zero-mean random variables with variance $1/N$, satisfies the RIP with a high probability as long as the number of rows is sufficient large.

- For *Case* 1, the sensing matrix $\mathbf{\Psi}$ is part of orthonormal basis $\mathbf{\Phi}$, the entries of which are zero-mean with variance $1/N$. Therefore, according to [72], the sensing matrix satisfies RIP with a high probability.

- For *Case* 2, we know from *Case* 1 that the entries in $\mathbf{\Phi}$ have zero mean and variance being equal to $1/N$, i.e., $\mathbb{E}(\tilde{\phi}_{i,j}) = 0$ and $\mathbb{E}(\tilde{\phi}_{i,j}^2) = 1/N$. Next, given that each element of the channel vector is zero-mean and unit-variance, we have $\mathbb{E}(h_{i,j}^k) = 0$ and $\mathbb{E}\left(\left(h_{i,j}^k\right)^2\right) = 1$. Then, since the orthonormal basis and the channel coefficients are independent, we know $\mathbb{E}(\Psi_{i,j}) = \mathbb{E}(\tilde{\phi}_{i,j} h_{i,j}^k) =$

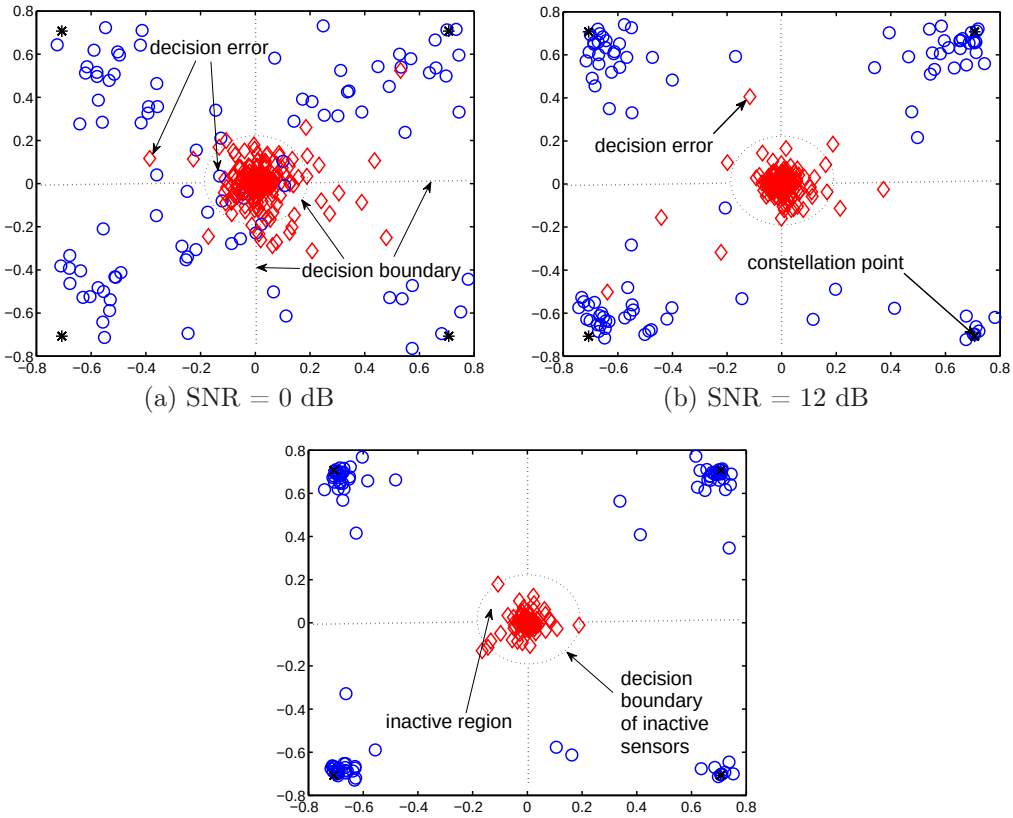

(a) SNR = 0 dB (b) SNR = 12 dB

(c) SNR = 24 dB

Figure 5.3: Reconstructed symbols in the constellation diagram of QPSK. The red diamond markers denote the reconstructed symbols from inactive sensors, the blue circle markers denote the reconstructed symbols from active sensors, and the dotted lines are the proposed decision boundaries.

$\mathbb{E}(\tilde{\phi}_{i,j})\mathbb{E}(h^k_{i,j}) = 0$ and $\mathbb{E}(\Psi^2_{i,j}) = \mathbb{E}\left(\tilde{\phi}^2_{i,j}\left(h^k_{i,j}\right)^2\right) = \mathbb{E}\left(\tilde{\phi}^2_{i,j}\right)\mathbb{E}\left(\left(h^k_{i,j}\right)^2\right) = 1/N$. Therefore, we have shown that the entries of $\mathbf{\Psi}$ have zero mean and variance $1/N$, which implies that $\mathbf{\Psi}$ satisfies RIP with a high probability.

- For *Case* 3, the sensing matrix is selected as the channel matrix itself, all the entries of which are Gaussian distributed. Thus, it satisfies RIP with a high probability according to [72].

For the general case where the path propagation loss is considered, the sensing matrix becomes the product of the sensing matrix in (5.6) and a basis (a diagonal

matrix with the diagonal entries being path loss). Such a sensing matrix also satisfies RIP according to [74].

5.3.4 The Impact of SNR on Reconstruction Error

To evaluate the impact of SNR on reconstruction performance, we derive the following property

Property 1. *Assume that the sensing matrix* $\mathbf{\Psi}$ *obeys RIP. Then, as the lowest SNR among all the active sensor nodes increases, the upper bound of the* l_2 *norm of the reconstruction error for the transmitted symbol decreases as* $\mathcal{O}(\mathsf{SNR}^{-1})$.

Proof: When the the sensing matrix $\mathbf{\Psi}$ obeys RIP, to be more specific, $\delta_{2r} < \sqrt{2}-1$, then the solution $\hat{\mathbf{x}}$ to problem (5.4) obeys [13]

$$\|\hat{\mathbf{x}} - \mathbf{x}\|_2 = \sqrt{\sum_{i=1}^{N} P_i(\hat{s}_i - s_i)^2} \leq C\varepsilon \approx C\sqrt{pM_cM_r}\sigma \tag{5.9}$$

for constant C, where σ is the standard deviation of the noise. There exists $\sqrt{P_k}$, satisfying $\sqrt{P_k} \leq \sqrt{P_l}$ for $\forall l \in (1, ..., N)$. Thus,

$$\sqrt{P_k}\|\hat{\mathbf{s}} - \mathbf{s}\|_2 \leq \|\hat{\mathbf{x}} - \mathbf{x}\|_2 \leq C\sqrt{pM_cM_r}\sigma. \tag{5.10}$$

Then we have

$$\|\hat{\mathbf{s}} - \mathbf{s}\|_2 \leq \frac{C\sqrt{pM_cM_r}}{\sqrt{\mathsf{SNR}}}. \tag{5.11}$$

where SNR is defined for sensor node i as P_i/σ^2. Therefore, the upper bound of $\|\hat{\mathbf{s}} - \mathbf{s}\|_2$ decreases when the worst SNR at the receiver among all the active users increases, which completes the proof. □

Having obtained the reconstructed symbol $\hat{\mathbf{s}}$ from the CS-based recovery, the next step is to design an appropriate decision boundary that maps the reconstructed sym-

bol $\hat{\mathbf{s}}$ to the constellation points. Fig. 5.3 illustrates the QPSK-modulated symbols under different SNRs for a network of $N = 100$ sensor nodes with $r = 10$ active sensors and single antenna at the receiver. The results in Fig. 5.3 are obtained via 10 simulations with sufficient number of observations. The blue circles represent the symbols reconstructed from the active sensors while the red diamonds are from the inactive sensors. In the ideal noise-free case, the blue circles should locate perfectly at the four constellation points while the red diamonds concentrate at the origin. Observed from Fig. 5.3 that as SNR increases, the reconstructed symbols are more accurately positioned at the desired positions, respectively. For example, the transmitted symbols can be recovered precisely when SNR reaches 24 dB.

Due to the reconstruction error in the recovery process, misplacement can occur for both types of points. In particular, depending on the SNR value, two types of decision errors are likely to occur. One is the traditional decision error that occurs in mapping the reconstructed symbols of the active sensors to the constellation points, which is referred to as Type-I error. On the other hand, an active (inactive) sensor can be mistakenly decided to be inactive (active) in the low SNR region (e.g., Fig. 5.3 (a)), which is referred to as Type-II error. To address the unique constellation mapping challenge, we propose here a novel decision boundary as shown by the dotted line in Fig. 5.3. In addition to the normal four-quadrant decision region for the QPSK-modulated symbols, a circle decision boundary is introduced centering the origin to properly handle the reconstructed symbols of the inactive sensors. To determine the circle decision boundary, we can first use one set of sparse training data with the identity information of the active sensors being known. After the CS reconstruction of these training data, based on the reconstructed symbols in the constellation diagram, we can find an appropriate decision boundary trying to reduce the decision errors.

As is mentioned above, Type-II decision errors are more likely to occur when the transmission SNR is low. In what follows, we explore temporal diversity and propose one effective remedy to eliminate type-II errors. Note that CS-based symbol recovery is performed in every symbol duration and there are multiple symbols in one data packet. Therefore, the decision results from multiple symbol time durations are made as "soft decision inputs" to a final decision module that employs a majority fusion rule. For example, if most of the symbols in a packet after constellation demapping are null symbols, the corresponding sensor is decided to be inactive.

Our work differs from [55] in that we have revealed the impact of communication SNR on CS-based MAC schemes from a physical layer perspective. In particular, it has been emphasized that CS-based recovery is applied on the symbol level rather than the actual environmental data. This critical observation has further enabled us to identify the unique decision challenge in distinguishing between active and inactive transmitters in the process of constellation demapping. Novel decision boundary as well as effective method have been proposed to enhance symbol recovery accuracy.

Note that in the proposed scheme, more data transmissions give the receiver (fusion center) more observations for successful CS reconstruction at the cost of more energy consumption. In practice, the receiver (or the fusion center) may often be equipped with electric power and thus can handle higher complexity while sensor nodes are often battery powered. For this reason, multiple antennas are employed at the receiver in our scheme to obtain more observations to save transmission power, which is beneficial for the whole sensor network as it effectively reduces the time period needed to collect sufficient number of observations for data recovery, thereby contributing positively to the lifetime extension of the transmitting nodes.

5.3.5 Perturbations in Compressed Sensing

In the previous sections, we have considered perturbed observations at the receiver caused by the measurement noise. In this section, we consider the perturbations to the sensing matrix $\mathbf{\Psi}$. We have discussed the sensing matrix selection before and we know that channel information is included within the sensing matrix. We assumed that the channel information is perfectly known at the receiver side and the CS reconstruction is based on the accurate knowledge of sensing matrix. However, in practice there always exists channel estimation error which causes perturbations to the sensing matrix.

The l_1 minimization problem **P1** can be generalized by incorporating a perturbed sensing matrix in the form of

$$\begin{aligned} \underset{\mathbf{x}}{\text{minimize}} \quad & \|\mathbf{x}\|_1 \\ \text{subject to} \quad & \|\mathbf{z} - (\mathbf{\Psi} + \mathbf{E})\mathbf{x}\|_2 \leq \varepsilon' \end{aligned} \tag{5.12}$$

for some $\varepsilon' \geq 0$, where $\mathbf{E}$ is the error matrix. Now we introduce two theorems summarized by [75].

Theorem 1. Given the isometry constant δ_r associated with matrix $\mathbf{\Psi}$, and the relative perturbation $\varepsilon^{(r)}$ which is denoted as $\frac{\|\mathbf{E}\|_2^{(r)}}{\|\mathbf{\Psi}\|_2^{(r)}} \leq \varepsilon^{(r)}$, where $\|\cdot\|_2^{(r)}$ is the spectral norm of submatrices consisting of an arbitrary collection of r columns. Fix the constant

$$\hat{\delta}_{r,max} = (1 + \delta_r)(1 + \varepsilon^{(r)})^2 - 1. \tag{5.13}$$

Then the isometry constant $\hat{\delta}_r \leq \hat{\delta}_{r,max}$ for matrix $\mathbf{\Psi} + \mathbf{E}$ is the smallest nonneg-

ative number such that

$$(1-\hat{\delta}_r)\|\mathbf{x}\|_2^2 \leq \|(\mathbf{\Psi}+\mathbf{E})\mathbf{x}\|_2^2 \leq (1+\hat{\delta}_r)\|\mathbf{x}\|_2^2 \tag{5.14}$$

holds for all r-sparse vectors $\mathbf{x}$.

Before introducing the next theorem let us define the following constants associated with matrix $\mathbf{\Psi}$

$$\alpha = \frac{\|\mathbf{\Psi}\|_2}{\sqrt{1-\delta_r}}, \quad \beta^{(r)} = \frac{1+\delta_r}{1-\delta_r}. \tag{5.15}$$

Also introduce the relative bounds

$$\frac{\|\mathbf{E}\|_2}{\|\mathbf{\Psi}\|_2} \leq \varepsilon, \quad \frac{\|\mathbf{W}\|_2}{\|\mathbf{z}\|_2} \leq \varepsilon_w. \tag{5.16}$$

Theorem 2. Fix the relative bounds ε, $\varepsilon^{(r)}$, $\varepsilon^{(2r)}$ and ε_w. Assume the isometry constant for $\mathbf{\Psi}$ satisfies

$$\delta_{2r} < \frac{\sqrt{2}}{(1+\varepsilon^{(2r)})^2} - 1. \tag{5.17}$$

Then the solution of the BP problem (5.12) obeys

$$\|\hat{\mathbf{x}} - \mathbf{x}\|_2 \leq C'(\beta^{(r)}\varepsilon^{(r)} + \varepsilon_w)\|\mathbf{z}\|_2, \tag{5.18}$$

where $C' = \frac{4\sqrt{1+\delta_{2r}}(1+\varepsilon^{(2r)})}{1-(\sqrt{2}+1)[(1+\delta_{2r})(1+\varepsilon^{(2r)})^2-1]}$.

From this theorem, we can see that the upper bound of the reconstruction error in this case is decided by the channel estimation error. It is straightforward that larger channel estimation error leads to larger upper bound of the CS reconstruction error. We will show this in the simulation results.

5.4 Compressed Sensing for Network Data Recovery

The data measurement acquired from sensing natural phenomena have compressible (sparse) representation in the frequency or the wavelet domain. In other words, DFT and DWT of the sensor readings $\mathbf{d}$ can be sparse. For example, the data of the temperature sensor readings provided by the Intel Berkeley Research lab over a period of one month [76] exhibits both sparsity in the frequency domain (by examining the readings from all the sensor nodes at one time instant) and sparsity in the wavelet domain[6] (by examining the data readings from one sensor node in consecutive time intervals) as shown in [58]. Hence, compressed sensing can be utilized to recover both the spatially and temporally correlated data measurements. In network data recovery part of the wireless sensor network, the fusion center utilizes further spatial and temporal correlations to recover the readings from all the sensor nodes over a number of consecutive time frames.

5.4.1 Utilizing Sparsity from Spatial Correlation

Suppose by the end of frame l, the data measurement vector from the active sensor nodes $\mathbf{d}_{\mathcal{A}}(l)$ has been successfully received via communication, which is given by

$$\mathbf{d}_{\mathcal{A}}(l) = \mathbf{U}(l)\mathbf{d}(l) = \mathbf{U}(l)\mathbf{F}^{-1}\mathbf{b}(l), \tag{5.19}$$

where $\mathbf{U}(l) \in \mathbb{R}^{r\times N}$ contains r randomly selected rows of identity matrix representing the address information of the active sensor nodes, $\mathbf{F}^{-1}$ represents the inverse DFT matrix and $\mathbf{b}(l)$ is the DFT of $\mathbf{d}(l)$. Since the readings of the sensors have spatial correlation due to closeness of the sensors, $\mathbf{b}(l)$ is sparse. In the network data recovery

[6]These data readings can also be sparse in frequency domain. Basically, smooth signals are more likely to be sparse in frequency domain and piecewise smooth signals are more likely to be sparse in wavelet domain.

part, compressed sensing is applied to reconstruct all the sensor data in the l-th time frame $\mathbf{d}(l)$ based on the active sensor data vector $\mathbf{d}_{\mathcal{A}}(l)$ obtained in communication part.

As such, the receiver can solve the following BP problem

$$\begin{aligned} \mathbf{P2} \quad & \underset{\mathbf{b}(l)}{\text{minimize}} \quad \|\mathbf{b}(l)\|_1 \\ & \text{subject to} \quad \mathbf{d}_{\mathcal{A}}(l) = \mathbf{U}(l)\mathbf{F}^{-1}\mathbf{b}(l). \end{aligned} \tag{5.20}$$

The data vector $\mathbf{d}(l)$ can be recovered with overwhelming probability if the number of measurements r is larger than the required number of observations m_s, which is obtained according to the spatial sparsity of the sensor readings r_s.

However, due to the randomness of r and the packet error[7] during the wireless communication, the actual obtained number of measurements could be less than m_s. In such a case, the recovered data vector $\mathbf{d}(l)$ will be inaccurate. To solve this problem, when $r < m_s$, the obtained active sensor data in time frame l will be stored at the receiver for use in the future. We note that selecting larger transmission probability λ may increase the number of observations r for network data recovery of all sensors in (5.20). Nevertheless, this brings about extra costs in terms of power consumption in two aspects. On the one hand, larger λ apparently leads to higher power consumption from the larger number of active sensor nodes. On the other hand, the rise in the number of the active sensor nodes increases the sparsity of $\mathbf{x}$ in (5.4), leading to more transmissions required for active sensor nodes.

To prove that the sensing matrix in problem **P2** obeys RIP, we note that the sensing matrix is a product of a subset of an identity matrix, $\mathbf{U}$, with an inverse DFT matrix, $\mathbf{F}^{-1}$. Given that the DFT transformation matrix is an orthogonal matrix, its inverse $\mathbf{F}^{-1}$ is an orthogonal matrix as well. Then, it follows from [73, Theorem 3.1]

[7]Cyclic redundancy check (CRC) is included for CS-MAC to reduce packet error rate.

and [77] that a uniformly sampled sub-orthogonal matrix $\mathbf{UF}^{-1}$ from an orthogonal matrix $\mathbf{F}^{-1}$ obeys RIP with a high probability when the number of measurements m is on the order of $r \log^4 N$.

5.4.2 Utilizing Sparsity from Temporal Correlation

There are two scenarios that could lead to the infeasible data recovery in **P2**. One is from the failure of accurate symbol recovery in communication, due to, e.g., the random channel fading, thermal noise, or insufficient number of observations of $\mathbf{z}$. The other is when the recovered number of active sensor observations r is less than m_s for successful network data recovery of all sensors. The purpose of this section is to address the aforementioned recovery failures by utilizing the time correlations of the data measurements.

Suppose after K time frames, the number of successfully recovered data packets originated from sensor i equals $K_i < K$. Denote the corresponding set of *success* frame index for the i-th sensor as $\mathcal{B}_i = \{b_1, ..., b_{K_i}\}$ and the corresponding recovered data measurements vector as $\mathbf{t}_i = [d_i(b_1) \cdots d_i(b_{K_i})]$. We have

$$\mathbf{t}_i = \mathbf{U}_i \mathbf{d}_i = \mathbf{U}_i \mathbf{W}^{-1} \mathbf{v}_i \tag{5.21}$$

where $\mathbf{d}_i = [d_i(1) \cdots d_i(K)]^T$ denotes the data vector of sensor node i in K consecutive time frames, $\mathbf{U}_i \in \mathbb{R}^{K_i \times K}$ contains K_i randomly selected rows of identity matrix representing the index of the time frame during which the sensor readings of sensor node i are successfully recovered in the first or second steps, $\mathbf{W}^{-1}$ represents an orthogonal inverse DWT matrix and $\mathbf{v}_i$ is the DWT of $\mathbf{d}_i$. Since the readings of one sensor in consecutive time frames have temporal correlation due to the smooth variations of the real world signal, $\mathbf{v}_i$ is sparse. To recover the data of sensor node i

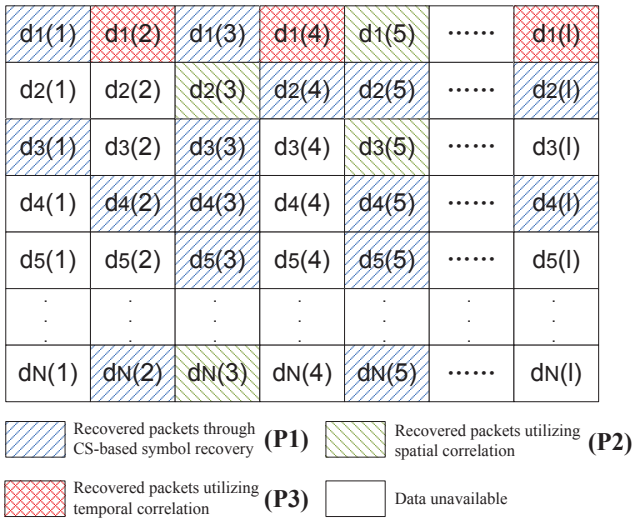

Figure 5.4: The data recovery process utilizing spatial and temporal correlations.

in all K frames, the receiver can solve the following BP problem

$$\begin{aligned} \mathbf{P3} \quad & \underset{\mathbf{v}_i}{\text{minimize}} \quad \|\mathbf{v}_i\|_1 \\ & \text{subject to} \quad \mathbf{t}_i = \mathbf{U}_i \mathbf{W}^{-1} \mathbf{v}_i \end{aligned} \tag{5.22}$$

Again, the data $\mathbf{d}_i$ can be recovered with overwhelming probability if K_i is not less than the required number of observations m_t which can be obtained according to the data sparsity from the time correlation. Note that the sensing matrix $\mathbf{U}_i\mathbf{W}^{-1}$ obeys RIP, the proof of which can be made similar to that of the DFT case in Section 5.4.1.

To better illustrates the data recovery process utilizing both spatial and temporal correlations, an example has been shown in Fig. 5.4. Each column represents the data packets transmitted by all the sensor nodes in a certain time frame while each row represents the data packets from a certain sensor node over l time frames. The blue shadowed data packets are the ones of the active sensor nodes that are successfully recovered in the communication process (i.e., **P1** in (5.4)), and the unshadowed

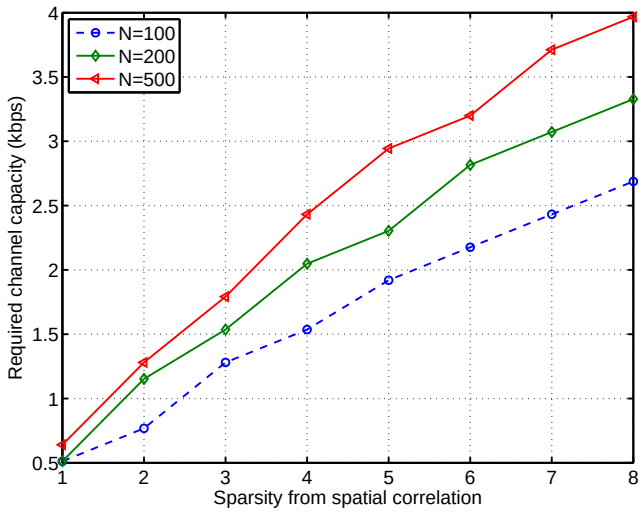

Figure 5.5: Required channel capacity versus sparsity from spatial correlation (N being the total number of sensors, $T_f = 1\,\mathrm{s}$).

packets represent the unavailable data. The green shadowed data packets are those recovered utilizing spatial correlation (i.e., **P2** in (5.20)). As can be observed from Fig. 5.4, in the third and fifth time frames, all the data of N sensors are obtained after CS recovery in the first two steps (**P1** and **P2**). The red shadowed packets are those recovered utilizing temporal correlation (i.e., **P3** in (5.22)), and it can be seen that all the data packets of sensor node 1 are obtained after utilizing 3-step CS recovery (**P1**-**P3**). Those red shadowed packets obtained utilizing temporal correlation can be further used as additional measurements for spatial domain CS recovery (**P2**) (e.g., the second and l th time frame in Fig. 5.4). By successively utilizing spatial and temporal correlation, all the data packets of the network over a period of time could be recovered.

5.5 Simulation Results

Simulation results are provided in this section. We consider a wireless sensor network consisting of N sensor nodes in a frequency-flat Rayleigh fading environment with

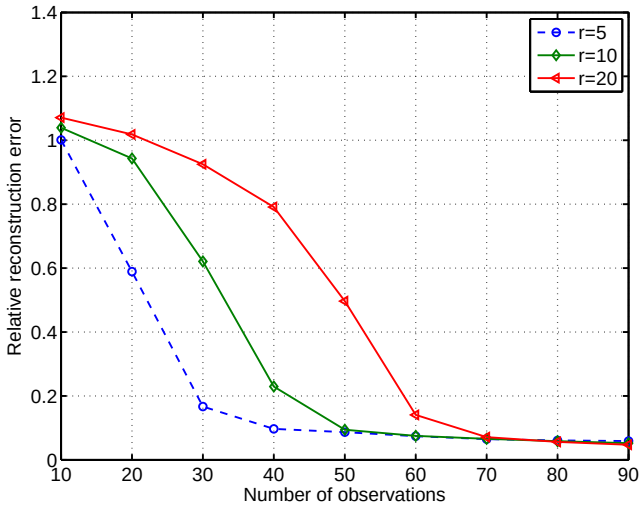

Figure 5.6: The relative reconstruction error versus number of observations for different number of active users (r being the number of active sensors, $T_f = 1\,\text{s}$, and SNR $= 32\,\text{dB}$).

channel coefficients having zero mean and unit variance. The number of receiving antennas $M_r = 4$ at the receiver. Unless stated otherwise, the number of sensor nodes $N = 100$ and the channel coefficients are assumed to remain unchanged during one time frame and the degree of freedom $M_c = 1$. The duration of one time frame $T_f = 1\,\text{s}$, the length of each sensing data packet L is set to 128 bits, the physical layer data rate $R = 3.2\,\text{kbps}$, and the modulation scheme is QPSK. Thus, a packet length of 128 bits containing 64 symbols are transmitted in one time frame, and the number of time slots in one time frame is $I = 25$. The DWT matrix used in simulations is an orthonormal matrix based on Daubechies wavelets.

5.5.1 Reconstruction Performance of the Proposed CS-based Scheme

Fig. 5.5 shows the required channel capacity versus the sparsity of the sensor data from spatial correlation for different total number of sensor nodes N. The required channel capacity is obtained based on the required number of active sensor nodes as

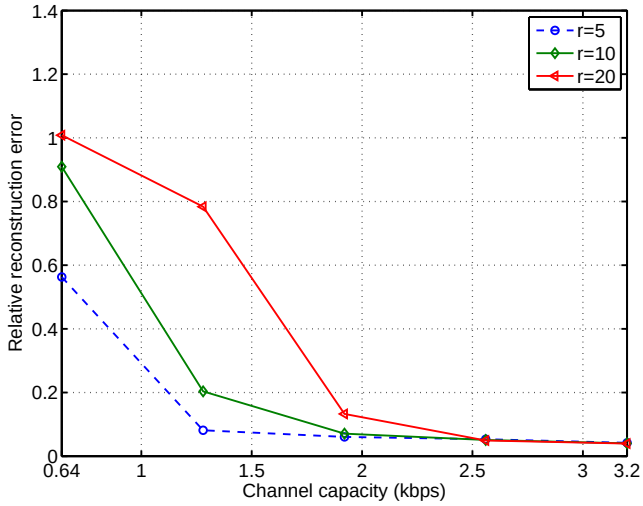

Figure 5.7: The relative error of reconstruction versus channel capacity ($T_f = 1\,\mathrm{s}$ and $\mathrm{SNR} = 32\,\mathrm{dB}$).

indicated in Section 5.3 ($C = Lr/T_f$). From this figure, we can see that as sparsity from spatial correlation increases, the required channel capacity almost grows linearly. It also can be seen that larger channel capacity is required for large total number of sensor nodes (e.g., $N = 500$ in Fig. 5.5) with fixed sparsity from spatial correlation.

Fig. 5.6 shows the average relative reconstruction error of the transmitted symbols versus the number of observations as the number of active sensor nodes (i.e., sparsity r) increases from 5 to 20. The relative reconstruction errors is defined as $\|\hat{\mathbf{s}}-\mathbf{s}\|_2/\|\mathbf{s}\|_2$ and the SNR is set to 32 dB. It can be observed that as sparsity increases, the number of observations required to achieve the same reconstruction performance grows saliently. For example, while 40 observations are needed to achieve a relative reconstruction error of 10 % for sparsity $r = 5$, the required number of samples rises to 50 for $r = 10$ and to as large as 70 for $r = 20$. Besides, Fig. 5.6 also shows that as long as the number of observations is sufficiently large, the signal "degree of sparsity"[8] has no significant impact on the relative reconstruction performance.

Fig. 5.7 shows the average relative reconstruction error of the transmitted symbols

[8]The degree of sparsity is defined as the number of non-zero components in the corresponding signal vector.

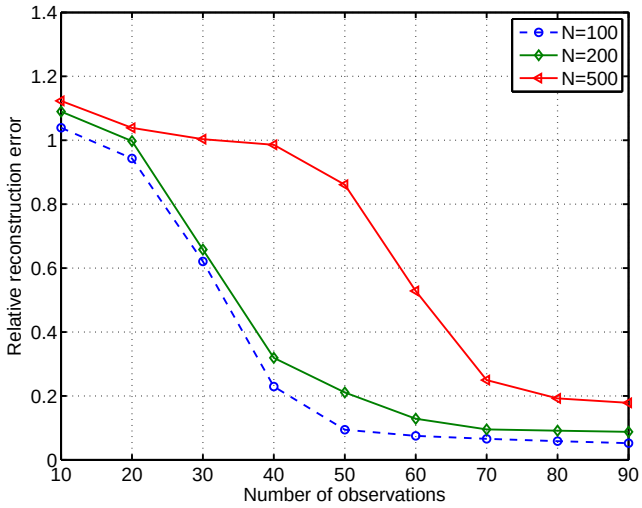

Figure 5.8: The relative reconstruction error versus number of observations for different total number of sensor nodes (N being the total number of sensors, $T_f = 1\,\text{s}$, $r = 10$, and SNR $= 32\,\text{dB}$).

versus the channel capacity as the number of active sensor nodes increases from 5 to 20. Here we change the physical layer data rate R to adjust the channel capacity and the the required the number of observations is set to $4r$. It can be observed that as sparsity increases, larger channel capacity is required to achieve the best reconstruction performance. With a channel capacity of about 1.3 kbps, the transmitted symbols can be successfully recovered for $r = 5$, while 2.6 kbps is required for $r = 20$.

Fig. 5.8 shows the average relative reconstruction error of the transmitted symbols versus the number of observations as the total number of sensor nodes N increases. It can be seen that as N increases, the required number of observations to achieve the same reconstruction performance grows significantly. For instance, to achieve a relative reconstruction error of 0.2, about 40 observations are required for $N = 100$, while 80 observations are required for $N = 500$. It also can be seen that the best reconstruction performance for large total number of sensor nodes is worse than that of small total number of sensors.

Fig. 5.9 illustrates the reconstructed QPSK symbols in constellation diagram when

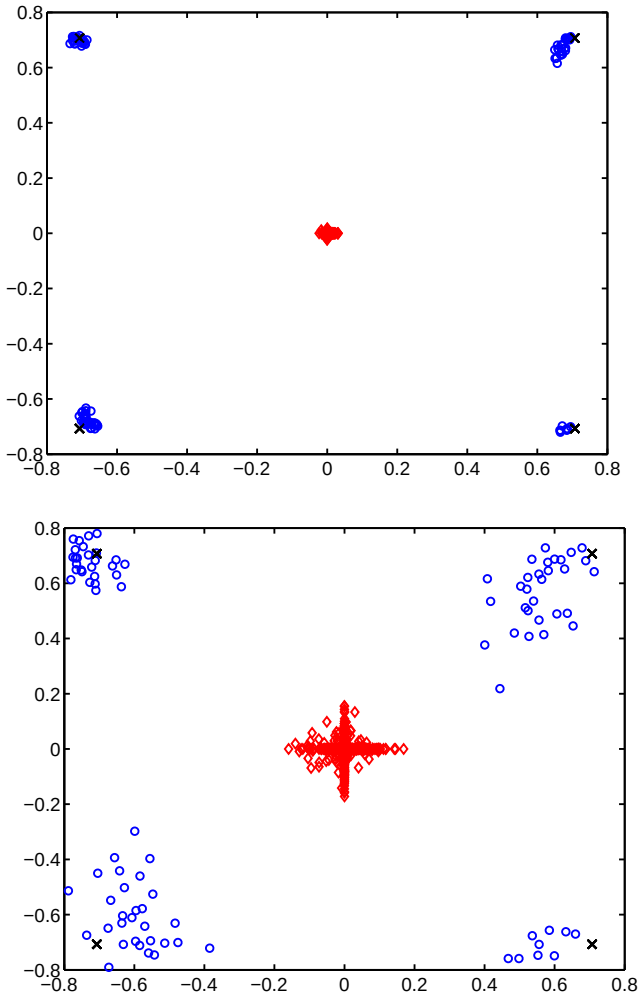

(b) Imperfect channel ($e \sim \mathcal{N}(0, 0.01)$)

Figure 5.9: Reconstructed symbols in the constellation diagram of QPSK while utilizing channel as the sensing matrix with SNR = 24 dB. The red diamond markers denote the reconstructed symbols from inactive sensors and the blue circle ones the symbols from active sensors.

the wireless channel is used as the sensing matrix. Here, the channel is assumed to have $M_c = 10$ degree of freedom (subchannels) that are independent and identically distributed (i.i.d.) with each subchannel varying independently in different time slots. The communication SNR is assumed to be 24 dB, $M_r = 4$, and other simulation parameters are identical to those of Fig. 5.3. We note that the reconstructed symbols are more accurately aligned at the constellation points compared with Fig. 5.3 (c).

Nevertheless, we would expect the performance gain to degrade in a correlated channel fading environment in either time or frequency. Besides, observe from Fig. 5.9 (b) that imperfect channel estimation at the receiver side also affects constellation mapping negatively.

5.5.2 Throughput Performance of the Proposed CS-Based Scheme

Comparison with CSMA

In this section, we conduct a comparative study of the throughput performance of CS-based multiple access and that of CSMA. In this comparison, CSMA is based on IEEE 802.11 distributed coordination function (DCF) with transmitting request to send (RTS) and clear to send (CTS) mechanisms [78]. The time slot for CSMA is assumed to equal symbol time duration, and the minimum and maximum contention windows are set to be $CW_{min} = 4$ and $CW_{max} = 64$, respectively. At the beginning, each active sensor senses the channel and will wait for a random backoff time (multiples symbol time durations) if the channel is not idle and start data transmission otherwise. Once the data packet has been correctly received at the receiver, an acknowledgement (ACK) signal will be sent back to the transmitter. If the transmitter does not receive the ACK within an acknowledgement period, e.g., due to collision or channel impairment, it will wait for another random backoff time to retransmit.

For the CS-based scheme, the maximum number of time slots in one time frame is $I = 25$, which ensures sufficiently large number of observations for CS-based symbol recovery. Taking into account communication errors, the maximum number of successfully received data packets during one time frame equals $r\times$ PER, where PER denotes the packet error rate. For a fair comparison, necessary transmission overhead are considered for CSMA. To be specific, 96 bits are added incorporating the identity information, RTS, CTS. Besides, an extra 32 bits ACK frame is also included

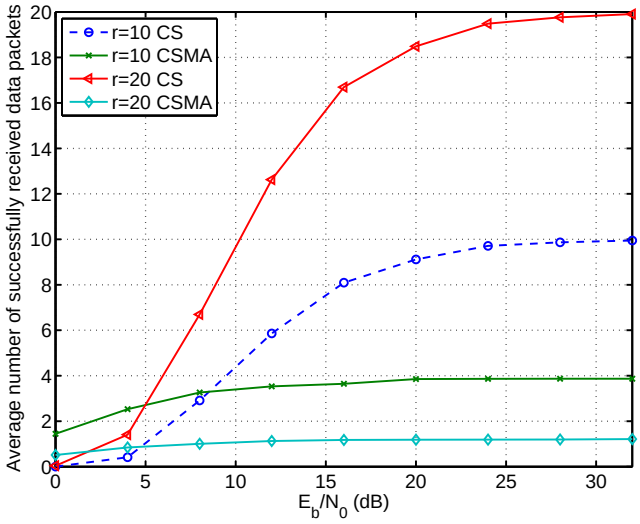

Figure 5.10: Average number of active sensor data packets successfully received per frame versus SNR for different access schemes (r being the number of active sensors and $T_f = 1\,\mathrm{s}$).

for packet reception acknowledgement. Hence, the maximum number of time slots in one time frame for CSMA is $I_{CSMA} = RT_f \times 128/L_{CSMA} = 1600$. Finally, the number of successfully received data packets for CSMA can be obtained with p_b, where $p_b = \frac{1}{2}\mathrm{erfc}(\sqrt{\frac{|h_i|^2 E_b}{N_0}})$ is the bit error rate (BER) for QPSK modulated signal in Rayleigh fading channel [79], E_b the value of bit energy, and h_i the channel fading coefficient for the i-th sensor node.

Fig. 5.10 shows the average number of successfully received active sensor data packets in one time frame versus SNR with sparsity being equal to 10 and 20, respectively. It is evident that SNR affects the throughput performance of both CSMA and CS-based MAC schemes positively. The impact, however, is much more salient on the CS-based scheme. For example, as SNR increases, the number of received data packets of CSMA quickly saturates while that of the CS-based scheme increments gradually in a much wider range. In other words, the performance of CS-based scheme is more sensitive to SNR variations. It is also worth noting that there exists a maximum achievable throughput upper bound for CSMA. For example, CSMA is only able to

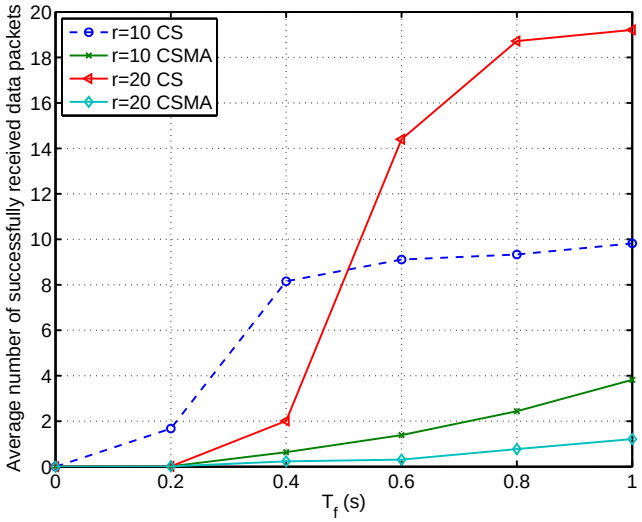

Figure 5.11: Average number of active sensor data packets successfully received per frame versus duration of one time frame for different access schemes in fading channel (r being the number of active sensors and SNR = 24 dB).

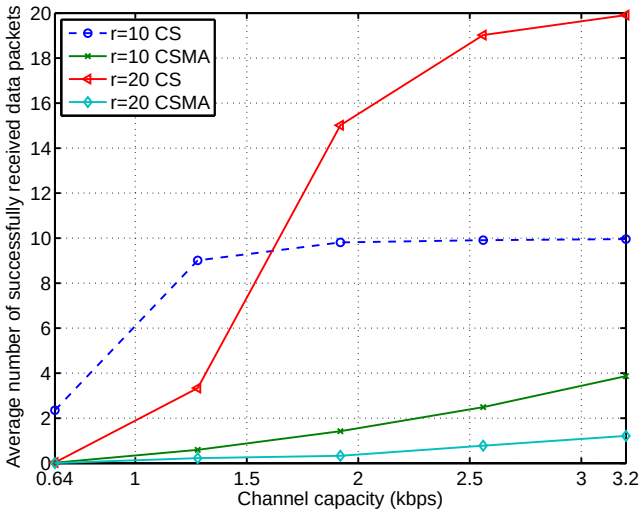

Figure 5.12: Average number of active sensor data packets successfully received per frame versus channel capacity for different access schemes (T_f = 1 s and SNR = 32 dB).

deliver about 4 data packets for the case of $r = 10$ in the simulation specific setting. In contrast, the CS-based MAC scheme is able to accommodate more simultaneous transmissions as long as the number of observations are sufficiently large.

Next, we compare in Fig. 5.11 the average number of successfully received data

packets of CS-based scheme with CSMA for different frame length T_f, and the SNR is set to 24 dB. We know that for fixed data rate R and packet length L, the maximum number of time slots in one time frame I and I_{CSMA} is linearly proportional to T_f. Then, it is observed from Fig. 5.11 that both schemes perform poorly when the frame length T_f is less than 0.2 s. In this case, for the CS-based scheme, the number of time slots I is not large enough for successful CS recovery. While for CSMA, I_{CSMA} is too small such that only limited number of sensor nodes are granted the opportunity to transmit. As the frame length increases, the average number of received data packets for the CS-based scheme grows rapidly and peaks around the maximum value while that of CSMA can only achieve around 4 when $r = 10$, and 1 when $r = 20$.

Fig. 5.12 shows the average number of successfully received active sensor data packets in one time frame versus channel capacity with sparsity being equal to 10 and 20, respectively. For CS reconstruction, smaller channel capacity leads to less observations for reconstruction while for CSMA, smaller channel capacity leads to less time slots in one time frame. It is observed that both access schemes have poor performance when channel capacity is around 0.64 kbps. However, as channel capacity increases, the average number of received data packets for the CS-based scheme grows rapidly which is similar to the performance in Fig. 5.11 while that of CSMA can only achieve a relatively small value.

5.5.3 CS-Based Data Recovery Utilizing Both Temporal and Spatial Correlations

Finally, we illustrate the reconstruction performance of the whole sensor network over a time period when temporal and spatial correlations are jointly explored. The sensor reading data we used is based on the data provided by [76]. Therefore, according to the experiment settings provided by [76], the geographical field is two dimension

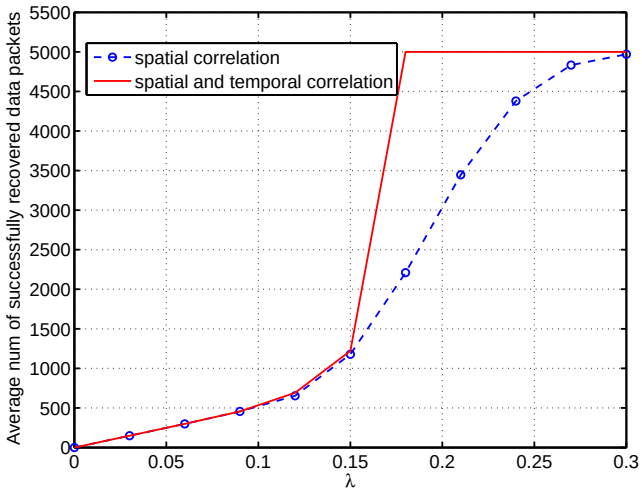

Figure 5.13: Average number of network data packets successfully recovered utilizing spatial correlation and utilizing both spatial and temporal correlation with different λ.

and approximately equally spaced. Without loss of generality, a total time period of $K = 50$ time frames are considered with the required number of observations $m_s = 20$ and $m_t = 20$. Fig. 5.13 illustrates the average number of successfully recovered data packets utilizing spatial and temporal correlations with different λ in the high SNR regime (communication error has been ignored). The dotted circle line represents the recovery scheme using only spatial correlation while the solid line represents that using both temporal and spatial correlations. From Fig. 5.13 we observe that the number of recovered network data packets for both schemes increases with the access probability λ. In particular, the joint scheme exhibits a surge in the number of recovered data packets when λ exceeds a threshold of around 0.15. This implies that to recover the same number of data packets, the joint scheme requires smaller value of λ, or, less number of active sensor nodes, which translates further to the reduced power consumption for the whole system.

5.6 Conclusions

This chapter has elaborated the role of compressed sensing in wireless sensor networks in terms of medium access and data reconstruction. A CS-based multiple access scheme that exploits sparsity in the process of medium access, as well as the spatial and time correlations that exist in natural signals has been proposed. To the best of our knowledge, our work made the first attempt in studying the impact of communication SNR on the accuracy of CS-based transmission symbol recovery, as well as the role of fading channel coefficients in sensing matrix selection. A novel decision boundary has been proposed to address the problem of distinguishing between active and inactive transmitters after symbol recovery. In the comparison between CSMA and the proposed CS-based scheme, we have found that increasing communication SNR enhances the throughput of both CSMA and CS-based schemes. Moreover, CS-based scheme is able to accommodate more simultaneous transmissions than CSMA. Finally, we have demonstrated the virtue of utilizing spatial and temporal correlations in recovering data measurements of the whole network.

Chapter 6

Conclusions and Future Research

6.1 Conclusions

Two research problems have been modeled and analyzed in the thesis: resource allocation problem for cognitive radio networks and multiple access for wireless sensor networks. For CR networks, a general resource allocation framework has been proposed and several spectrum access methods are utilized adaptively to enhance the energy efficiency employing both spectrum and spatial opportunities. For wireless sensor networks, compressed sensing theory has been used to propose a novel multiple access scheme, as well as a new scheme for network data recovery. Compared with the current technologies, these new methods can significantly improve system performance.

One of the main contributions of the thesis is that it unifies existing resource allocation methods for CR networks into a general framework, and adaptively utilizes the spectrum resource based on the location information of the secondary users. This approach intelligently utilizes frequency and space opportunities and minimizes the overall power consumption while maintaining the quality of service of the primary system. Specifically, the single SU case has been considered in Chapter 2, and spec-

trum access methods were utilized adaptively according to the location of the SU. In Chapter 3, the multiple SUs case has been investigated and two novel algorithms have been proposed to solve the resource allocation problem and to save energy for spectrum sensing meanwhile. Due to the uncertainty present in the CR-to-PU channel, a robust interference constraint with channel uncertainty has been imposed to protect the PU system in Chapter 4, and two optimization approaches were discussed to solve the power consumption problem. The simulation results show that there exists a tradeoff between energy efficiency and protection for primary user: when the interference constraint is tight, more power is required to achieve the minimum data requirement.

Another main contribution of this thesis is the application of the compressed sensing theory for multiple access and network data recovery of wireless sensor networks. In Chapter 5, we have described the complete CS-based symbol recovery process in a multiple access channel and investigated the impact of SNR on the accuracy of the CS-based transmission symbol recovery. For the CS reconstruction, we not only considered the perturbed observations at the receiver caused by the measurement noise, but also the perturbations to the sensing matrix. In addition, multiple antennas have been considered to be equipped at the receiver to increase the number of random projections observed by the receiver. In the existing CS-based MAC work, the sensor nodes have to retransmit their data if the number of observations is not sufficient for successful CS recovery. With multiple antennas at the receiver, the times of data retransmission can be reduced significantly. Finally, a detailed performance comparison between carrier sense multiple access (CSMA) and the proposed CS-based MAC has been performed. From the simulation results, we found that the CS-based scheme is able to accommodate more simultaneous transmissions than CSMA.

6.2 Recommendations for Future Research

The primary results of this thesis are for two research topics. Generally speaking, extension may be considered from the following aspects for the two topics.

6.2.1 Consider other structures for CR networks

The system model in this thesis is based on a scenario that one CR system coexists with one primary system, where the mobile SUs are communicating with the CBS in the uplink and the corresponding worst-case PUs receiving signals from the PBS. For the other network structures, such as mesh network in which the users communicate with each other in a distributed manner, the problem formulation and the method to solve the optimization problem can be totally different from that of this thesis. Location aware perspective, however, is still applicable, and can be explored in these network structures.

6.2.2 Consider other optimization objectives for CR networks

In this thesis, we formulated the optimization problem with the objective of minimizing the overall power consumption subject to a minimum data rate requirement. To achieve energy-efficient design, many recent research work take the energy efficiency minimization as the objective. In general, the optimization problems formulated in this thesis are convex problems while those problems taking the energy efficiency minimization as the objective are non-convex and hard to solve. Therefore, for future potential research, some novel algorithms can be proposed to solve such problems.

6.2.3 Consider resource allocation for CS-based wireless sensor networks in CR environments

The energy efficiency problem for CS-based cognitive radio WSNs has not been studied in this thesis. For a CS-based WSN in CR systems, only a fraction of the channels are available for the active sensors at one time slot, and the available channels change dynamically from one time slot to another. On the other hand, the number of the utilized channels is proportional to the number of the observations available for CS reconstruction. Thus, for future research a power strategy can be proposed to utilize the best available channels to transmit data, meanwhile, to ensure sufficient observations for CS reconstruction.

Appendix A

List of Publications

A.1 Journal Publications

[J1] **T. Xue**, X. Dong, and Y. Shi, "Resource Allocation Strategy for Multi-user Cognitive Radio Systems: Location-Aware Spectrum Access", submitted to *IEEE Transactions on Vehicular Technology*.

[J2] **T. Xue**, X. Dong, and Y. Shi, "Multiple access and data reconstruction in wireless sensor networks based on compressed sensing", *IEEE Transactions on Wireless Communications*, vol. 12, no. 7, pp. 3399–3411, July 2013.

[J3] **T. Xue**, Y. Shi, and X. Dong, "A framework for location-aware strategies in cognitive radio systems", *IEEE Wireless Communications Letters*, vol. 1, no. 1, pp. 30–33, February 2012.

A.2 Conference Publications

[C1] **T. Xue**, X. Dong, and Y. Shi, "A multiple access scheme based on multi-dimensional compressed sensing", *IEEE International Conference on Communications*, Ottawa, Ontario, Canada, June 2012.

Bibliography

[1] FCC, *Spectrum Policy Task Force*. Rep. ET Docket, 2002.

[2] S. Haykin, "Cognitive radio: brain-empowered wireless communications," *IEEE J. Sel. Areas Commun.*, vol. 23, no. 2, pp. 201–220, 2005.

[3] G. Staple and K. Werbach, "The end of spectrum scarcity," *IEEE Spectrum*, vol. 41, no. 3, pp. 48–52, Mar. 2004.

[4] A. Ghasemi and E. Sousa, "Spectrum sensing in cognitive radio networks: requirements, challenges and design trade-offs," *IEEE Commun Mag.*, vol. 46, no. 4, pp. 32–39, 2008.

[5] G. Ganesan and Y. Li, "Cooperative spectrum sensing in cognitive radio," *IEEE Trans. Wireless Commun.*, vol. 6, no. 6, pp. 2204–2222, 2007.

[6] Y. Zeng and Y.-C. Liang, "Eigenvalue-based spectrum sensing algorithms for cognitive radio," *IEEE Trans. Commun.*, vol. 57, no. 6, pp. 1784–1793, 2009.

[7] W.-Y. Lee and I. F. Akyildiz, "Optimal spectrum sensing framework for cognitive radio networks," *IEEE Trans. Wireless Commun.*, vol. 7, no. 10, pp. 3845–3857, 2007.

[8] T. Yucek and H. Arslan, "A survey of spectrum sensing algorithms for cognitive radio applications," *IEEE Commun. Surveys & Tutorials*, vol. 11, no. 1, pp. 116–130, 2009.

[9] E. Candes, J. Romberg, and T. Tao, "Robust uncertainty principles: Exact signal reconstruction from highly incomplete frequency information," *IEEE Trans. Inf. Theory*, vol. 52, no. 2, pp. 489–509, Feb. 2006.

[10] E. Candes and T. Tao, "Near optimal signal recovery from random projections: Universal encoding strategies?" *IEEE Trans. Inf. Theory*, vol. 52, no. 12, pp. 5406–5425, Dec. 2006.

[11] E. Candes, J. Romberg, and T. Tao, "Stable signal recovery from incomplete and inaccurate measurements," *Comm. Pure Appl. Math.*, vol. 59, no. 8, pp. 1207–1223, Aug. 2006.

[12] D. Donoho, "Compressed sensing," *IEEE Trans. Inf. Theory*, vol. 52, no. 4, pp. 1289–1306, Apr. 2006.

[13] E. Candes and M. Wakin, "An introduction to compressive sampling," *IEEE Signal Process. Mag.*, vol. 25, no. 2, pp. 21–30, Mar. 2008.

[14] W. Ye, J. Heidemann, and D. Estrin, "An energy-efficient MAC protocol for wireless sensor networks," in *Proc. IEEE Int. Conf. on Comput. Commun. (INFOCOM)*, vol. 3, 2002, pp. 1567–1576.

[15] T. v. Dam and K. Langendoen, "An adaptive energy-efficient MAC protocol for wireless sensor networks," in *Proc. Int. Conf. on Embedded Netw. Sensor Syst.*, vol. 1, 2003, pp. 171–180.

[16] L. Shi and A. O. Fapojuwo, "TDMA scheduling with optimized energy efficiency and minimum delay in clustered wireless sensor networks," *IEEE Trans. Mobile Comput.*, vol. 9, no. 7, pp. 927–940, 2010.

[17] Q. Gao, Y. Zuo, J. Zhang, and X. Peng, "Improving energy efficiency in a wireless sensor network by combining cooperative MIMO with data aggregation," *IEEE Trans. Veh. Technol.*, vol. 59, no. 8, pp. 3956–3965, Oct. 2010.

[18] G. G. d. O. Brante, M. T. Kakitani, and R. D. Souza, "Energy efficiency analysis of some cooperative and non-cooperative transmission schemes in wireless sensor networks," *IEEE Trans. Commun.*, vol. 59, no. 10, pp. 2671–2677, Oct. 2011.

[19] J. Matamoros and C. Antąäon-Haro, "Opportunistic power allocation and sensor selection schemes for wireless sensor networks," *IEEE Trans. Wireless Commun.*, vol. 9, no. 2, pp. 534–539, Feb. 2010.

[20] R. Yuan, T. Zhang, J. Huang, and L. Sun, "Opportunistic cooperation and optimal power allocation for wireless sensor networks," *IEEE Trans. Consumer Electronics*, vol. 56, no. 3, pp. 1898–1904, Aug. 2010.

[21] D. Grace, J. Chen, T. Jiang, and P. D. Mitchell, "Using cognitive radio to deliver green communications," *Proc. Int. Conf. Cognitive Radio Oriented Wireless Netw. and Commun. (CROWNCOM)*, pp. 1–6, Jun. 2009.

[22] J. Mitola, "Cognitive radio: an integrated agent architecture for software defined radio," Ph.D. dissertation, 2000.

[23] X. Zhou, G. Li, D. Li, D. Wang, and A. Soong, "Probabilistic resource allocation for opportunistic spectrum access," *IEEE Trans. Wireless Commun.*, vol. 9, no. 9, pp. 2870–2879, 2010.

[24] Y. Song and J. Xie, "Optimal power control for concurrent transmissions of location-aware mobile cognitive radio ad hoc networks," in *Proc. IEEE Global Telecommun. Conf. (Globecom)*, 2009, pp. 1–6.

[25] H. Celebi and H. Arslan, "Cognitive positioning systems," *IEEE Trans. Wireless Commun.*, vol. 6, no. 12, pp. 4475–4483, 2007.

[26] W. Chee, S. Friedland, and S. H. Low, "Spectrum management in multiuser cognitive wireless networks: optimality and algorithm," *IEEE J. Sel. Areas Commun.*, pp. 421–430, Feb. 2011.

[27] J. Wang and D. P. Palomar, "Worst-case robust MIMO transmission with imperfect channel knowledge," *IEEE Trans. Signal Process.*, no. 8, pp. 3086–3100.

[28] X. Kang, H. Garg, Y.-C. Liang, and R. Zhang, "Optimal power allocation for ofdm-based cognitive radio with new primary transmission protection criteria," *IEEE Trans. Wireless Commun.*, vol. 9, no. 6, pp. 2066–2075, 2010.

[29] A. Rabbachin, T. Q. S. Quek, H. Shin, and M. Z. Win, "Cognitive network interference," *IEEE J. Sel. Areas Commun.*, pp. 480–493, Feb. 2011.

[30] S. Boyd and L. Vandenberghe, *Convex Optimization.* Cambridge University Press, 2004.

[31] F. Meshkati, M. Chiang, H. V. Poor, and S. C. Schwartz, "A game-theoretic approach to energy-efficient power control in multicarrier CDMA systems," *IEEE J. Sel. Areas Commun.*, pp. 1115–1129, Jun. 2006.

[32] Q. Zhao and M. Sadler, B, "A survey of dynamic spectrum access," *IEEE Signal Process. Mag.*, vol. 24, no. 3, pp. 79–89, 2007.

[33] A. Ghasemi and E. S. Sousa, "Fundamental limits of spectrum-sharing in fading environments," *IEEE Trans. Wireless Commun.*, vol. 6, no. 2, pp. 649–658, Feb. 2007.

[34] L. B. Le and E. Hossain, "Resource allocation for spectrum underlay in cognitive radio networks," *IEEE Trans. Wireless Commun.*, vol. 7, no. 12, pp. 5306–5315, Dec. 2008.

[35] G. Bansal, M. J. Hossain, V. K. Bhargava, and T. Le-Ngoc, "Subcarrier and power allocation for OFDMA-based cognitive radio systems with joint overlay and underlay spectrum access mechanism," *IEEE Trans. Veh. Technol.*, vol. 62, no. 3, pp. 1111–1122, Mar. 2013.

[36] S. Wang, Z.-H. Zhou, M. Ge, and W. Chonggang, "Resource allocation for heterogeneous cognitive radio networks with imperfect spectrum sensing," *IEEE J. Sel. Areas Commun.*, vol. 31, no. 3, pp. 464–475, Mar. 2013.

[37] Y. Tachwali, B. F. Lo, I. F. Akyildiz, and R. Agusti, "Multiuser resource allocation optimization using bandwidth-power product in cognitive radio networks," *IEEE J. Sel. Areas Commun.*, vol. 31, no. 3, pp. 451–463, 2013.

[38] D. Shiung, Y.-Y. Yang, and C.-S. Yang, "Transmit power allocation for cognitive radios under rate protection constraints: a signal coverage approach," *IEEE Trans. Veh. Technol.*, vol. 59, no. 8, pp. 3956–3965, Oct. 2013.

[39] J. Zou, H. Xiong, D. Wang, and C. Chen, "Optimal power allocation for hybrid overlay/underlay spectrum sharing in multiband cognitive radio networks," *IEEE Trans. Veh. Technol.*, vol. 59, no. 8, pp. 3956–3965, Oct. 2013.

[40] J. Mao, G. Xie, J. Gao, and Y. Liu, "Energy efficiency optimization for OFDM-based cognitive radio systems: a water-filling factor aided search method," *IEEE Trans. Wireless Commun.*, vol. 99, no. 99, pp. 534–539, Oct. 2013.

[41] A. G. Marques, L. M. Lopez-Ramos, G. B. Giannakis, and J. Ramos, "Resource allocation for interweave and underlay crs under probability-of-interference constraints," *IEEE J. Sel. Areas Commun.*, vol. 30, no. 10, pp. 1922–1933, Nov. 2012.

[42] T. Xue, Y. Shi, and X. Dong, "A framework for location-aware strategies in cognitive radio systems," *IEEE Wireless Commun. Letters*, vol. 1, no. 1, pp. 30–33, Feb. 2012.

[43] W. Yu and R. Lui, "Dual methods for nonconvex spectrum optimization of multicarrier systems," *IEEE Trans. Commun.*, vol. 54, no. 7, pp. 1310–1322, 2006.

[44] D. Bertsekas, *Nonlinear Programming.* Belmont, MA: Athena Scientific, 1999.

[45] C. U. Saraydar, N. B. Mandayam, and D. J. Goodman, "Efficient power control via pricing in wireless data networks," *IEEE Trans. Commun.*, vol. 50, no. 2, pp. 291–303, Feb. 2002.

[46] A. G. Marques, E. Dall'Anese, and G. B. Giannakis, "Cross-layer optimization and receiver localization for cognitive networks using interference tweets," *IEEE J. Sel. Areas Commun.*, vol. 32, no. 3, pp. 641–653, Mar. 2011.

[47] S.-J. Kim, N. Y. Soltani, and G. B. Giannakis, "Resource allocation for OFDMA cognitive radios under channel uncertainty," *IEEE Trans. Wireless Commun.*, vol. 12, no. 7, pp. 3578–3587, 2013.

[48] S. Parsaeefard and A. R. Sharafat, "Robust distributed power control in cognitive radio networks," *IEEE Trans. Mobile Comput.*, vol. 12, no. 4, pp. 609–620, 2013.

[49] E. Dall'Anese, S.-J. Kim, G. B. Giannakis, and S. Pupolin, "Power control for cognitive radio networks under channel uncertainty," *IEEE Trans. Wireless Commun.*, vol. 10, no. 10, pp. 3541–3551, Oct. 2011.

[50] F. Chen, A. Chandrakasan, and V. Stojanovic, "Design and analysis of a hardware-efficient compressed sensing architecture for data compression in wireless sensors," *IEEE J. Solid-State Circuits*, vol. 47, no. 3, pp. 744–756, Mar. 2012.

[51] J. Tropp, J. Laska, M. Duarte, J. Romberg, and R. Baraniuk, "Beyond nyquist: effcient sampling of sparse bandlimited signals," *IEEE Trans. Inf. Theory*, vol. 56, no. 1, pp. 520–544, Jan. 2010.

[52] A. Dimakis, R. Smarandache, and P. Vontobel, "LDPC codes for compressed sensing," *IEEE Trans. Inf. Theory*, vol. 58, no. 5, pp. 3093–3114, May 2012.

[53] F. Fazel, M. Fazel, and M. Stojanovic, "Random access compressed sensing for energy-efficient underwater sensor networks," *IEEE J. Sel. Areas Commun.*, vol. 29, no. 8, pp. 1660–1670, Aug. 2011.

[54] S. Qaseem, T. Al-Naffouri, and A.-M. Tamim, "Compressive sensing based opportunistic protocol for exploiting multiuser diversity in wireless networks," in *Proc. IEEE Personal, Indoor and Mobile Radio Commun. Symp. (PIMRC)*, 2009, pp. 1447–1451.

[55] R. Mao and H. Li, "A novel multiple access scheme via compressed sensing with random data traffic," *J. Commun. Netw.*, vol. 12, no. 4, pp. 308–316, 2010.

[56] A. K. Fletcher, S. Rangan, and V. K. Goyal, "On-off random access channels: a compressed sensing framework," *Arxiv preprint*, 2009. [Online]. Available: http://arxiv.org/abs/0903.1022

[57] S. R. Bhaskaran, L. Davis, G. Alex, S. Hanly, and P. Tune, "Downlink scheduling using compressed sensing," in *IEEE Inf. Theory Workshop on Netw. and Inf. Theory (ITW 2009)*, 2009, pp. 201–205.

[58] T. Xue, X. Dong, and Y. Shi, "A multiple access scheme based on multi-dimensional compressed sensing," in *Proc. IEEE Int. Conf. on Commun. (ICC)*, 2012.

[59] M. Kaneko and A. A. Khaldoun, "Compressed sensing based protocol for efficient reconstruction of sparse superimposed data in a multi-hop wireless sensor network," *Arxiv preprint*. [Online]. Available: http://arxiv.org/abs/1208.1410

[60] R. Madan, S. Cui, S. Lall, and A. Goldsmith, "Cross-layer design for lifetime maximization in interference-limited wireless sensor networks," *IEEE Trans. Wireless Commun.*, vol. 5, no. 11, pp. 3142–3152, Nov. 2006.

[61] S. Cui, R. Madan, A. Goldsmith, and S. Lall, "Cross-layer energy and delay optimization in small-scale sensor networks," *IEEE Trans. Wireless Commun.*, vol. 6, no. 10, pp. 3688–3699, Oct. 2007.

[62] S. Cui, A. Goldsmith, and A. Bahai, "Energy-efficiency of MIMO and cooperative MIMO techniques in sensor networks," *IEEE J. Sel. Areas Commun.*, vol. 22, no. 6, pp. 1089–1098, Aug. 2004.

[63] Q. Gao, Y. Zuo, J. Zhang, and P. Xiaohong, "Improving energy efficiency in a wireless sensor network by combining cooperative MIMO with data aggregation," *IEEE Trans. Veh. Technol.*, vol. 59, no. 8, pp. 3956–3965, Oct. 2010.

[64] S. Marano, V. Matta, T. Lang, and P. Willett, "A likelihood-based multiple access for estimation in sensor networks," *IEEE Trans. Signal Process.*, vol. 55, no. 11, pp. 5155–5166, Nov. 2007.

[65] W. Bajwa, J. Haupt, A. Sayeed, and R. Nowak, "Compressive wireless sensing," in *Proc. Int. Conf. on Inf. Process. in Sensor Netw. (IPSN)*, 2006, pp. 134–142.

[66] B. Shahrasbi, A. Talari, and N. Rahnavard, "TC-CSBP: Compressive sensing for time-correlated data based on belief propagation," in *Proc. Annual Conf. on Inf. Sciences and Syst. (CISS)*, 2011, pp. 1–6.

[67] E. Candes and J. Romberg, "Sparsity and incoherence in compressive sampling," *Inverse Problems*, vol. 23, no. 3, pp. 969–985, Jun. 2007.

[68] S. Chen, D. Donoho, and M. Saunders, "Atomic decomposition by basis pursuit," *SIAM J. Sci. Comput.*, vol. 20, no. 1, pp. 33–61, 1999.

[69] *l_1-Magic, a collection of MATLAB routines for solving the convex optimization programs central to compressive sampling.* http://www.acm.caltech.edu/l1magic/.

[70] E. Candes and T. Tao, "Decoding by linear programming," *IEEE Trans. Inf. Theory*, vol. 51, no. 12, pp. 4203–4215, Dec. 2005.

[71] S. Mendelson, A. Pajor, and N. Tomczak-Jaegermann, "Uniform uncertainty principle for bernoulli and subgaussian ensembles," *Constr. Approx.*, vol. 28, no. 3, pp. 277–289, 2008.

[72] R. Baraniuk, M. Davenport, R. DeVore, and M. Wakin, "A simple proof of the restricted isometry property for random matrices," *Constr. Approx.*, vol. 28, no. 3, pp. 253–263, 2008.

[73] M. Rudelson and R. Vershynin, "On sparse reconstruction from fourier and gaussian measurements," *Comm. Pure Appl. Math.*, vol. 61, no. 8, pp. 1025–1045, 2008.

[74] V. Cevher, M. F. Duarte, and R. G. Baraniuk, "Distributed target localization via spatial sparsity," in *Proc. European Signal Process. Conf.*, 2008.

[75] M. A. Herman and T. Strohmer, "General deviants: An analysis of perturbations in compressed sensing," *IEEE J. Sel. Topics Signal Process.*, vol. 4, no. 2, pp. 342–349, Apr. 2010.

[76] S. Madden. http://db.csail.mit.edu/labdata/labdata.html, 2004.

[77] N. H. Nguyen and T. D. Tran, "Exact recoverability from dense corrupted observations via l_1 minimization," *Arxiv preprint*, 2011. [Online]. Available: http://arxiv.org/pdf/1102.1227.pdf

[78] G. Bianchi, "Performance analysis of the IEEE 802.11 distributed coordination function," *IEEE J. Sel. Areas Commun.*, vol. 18, no. 3, pp. 535–547, Mar. 2000.

[79] J. Proakis, *Digital Communications*. McGraw-Hill Science, Engineering, Math, 2000.